Performance of the Muon Detector for the LHCb Upgrade II

Phd student:
Francesco Debernardis

Supervisors:
Ch.mo Prof. Saverio Simone
Ch.ma Prof.ssa Alessandra Pastore
Ch.mo Prof. Marco Pappagallo

Coordinator:
Ch.mo Prof. Giuseppe Gonnella

PhD presentation
XXXVI cycle

11/04/2024

Outline

- Studies on the design of the LHCb muon detector at high luminosity
  - Rate estimate
  - Proposal of a new readout scheme
  - Dead time and muon ID

- Search for the rare decay mode $D_{s1}(2460)^+ \rightarrow {D_s}^+\mu^+\mu^-$
  - Optimisation of the D_s selection
  - $D_s^+\mu^+\mu^-$ selection
  - Observation of new decay modes

Outline

- Studies on the design of the LHCb muon detector at high luminosity
  - Rate estimate
  - Proposal of a new readout scheme
  - Dead time and muon ID

- Search for the rare decay mode $D_{s1}(2460)^+ \rightarrow {D_s}^+\mu^+\mu^-$
  - Optimisation of the D_s selection
  - $D_s^+\mu^+\mu^-$ selection
  - Observation of new decay modes

LHCb muon detector at Run 3

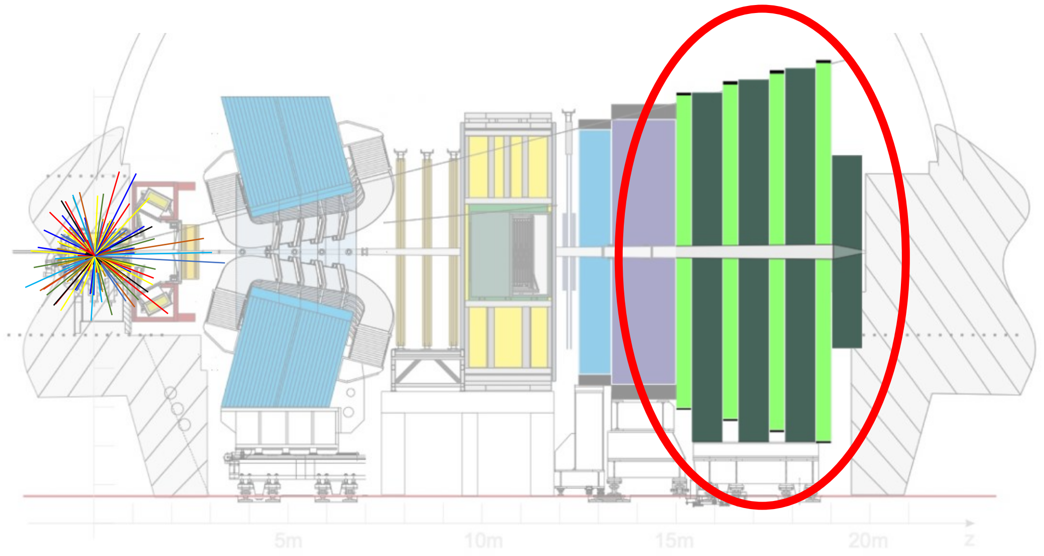

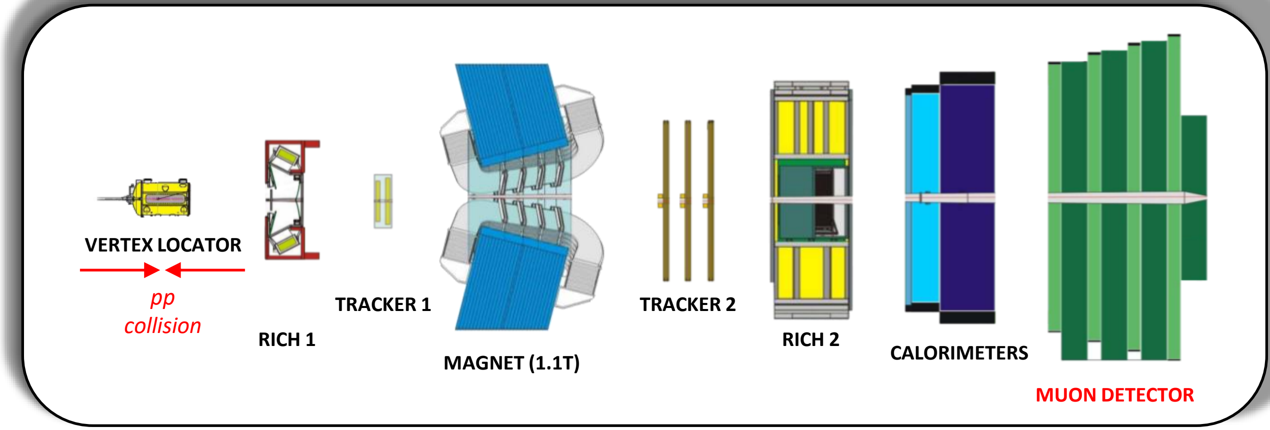

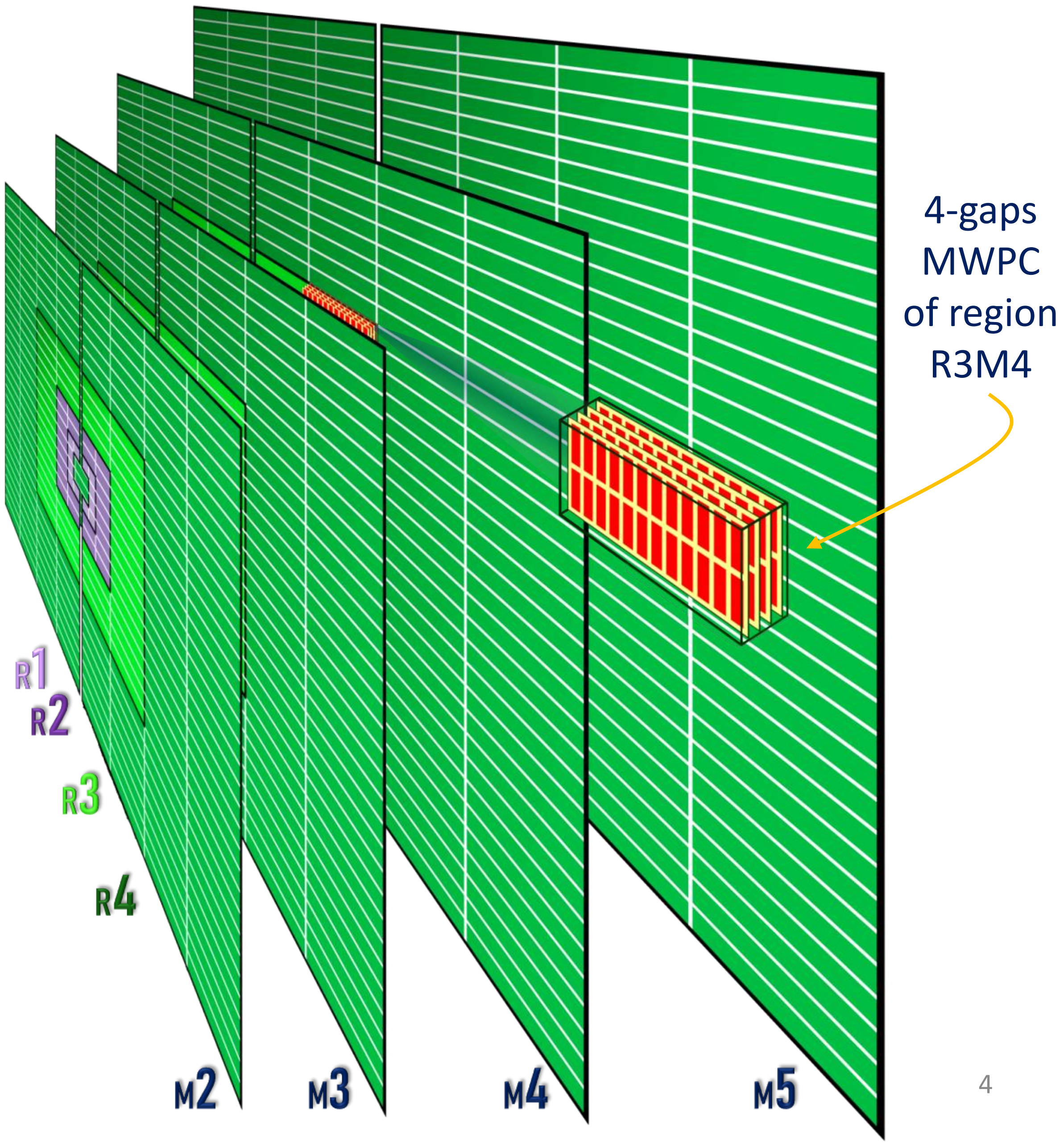

LHCb muon detector at Run 3

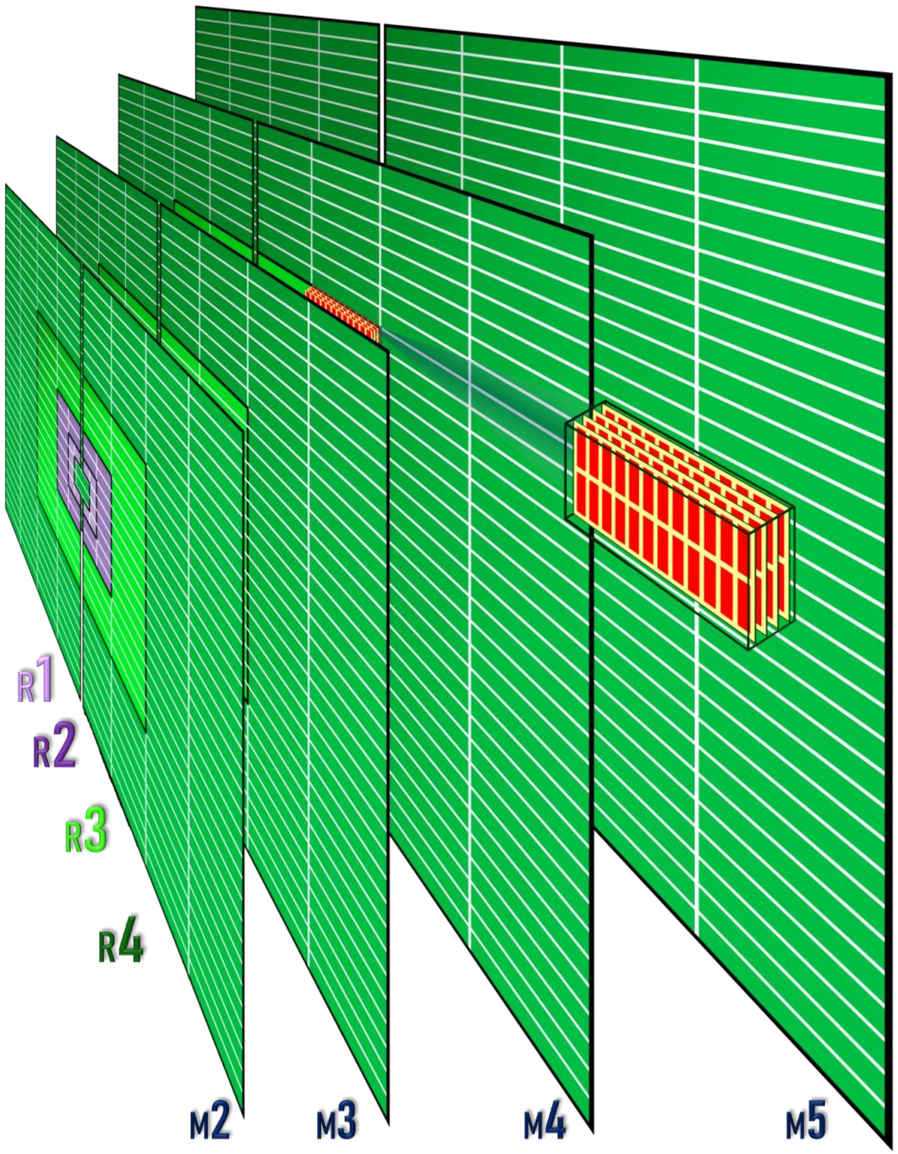

4 stations of 4-gaps multi-wire proportional chambers (MWPCs) with gas mixture Ar:CO_2:CF_4 (40:55:5). Iron absorbers 80 cm thick between stations

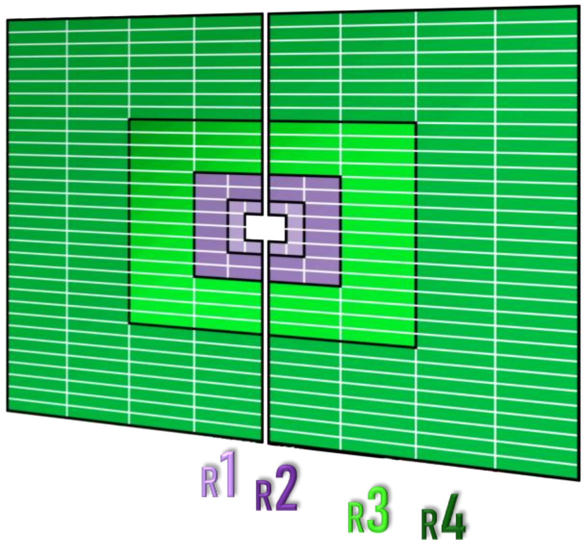

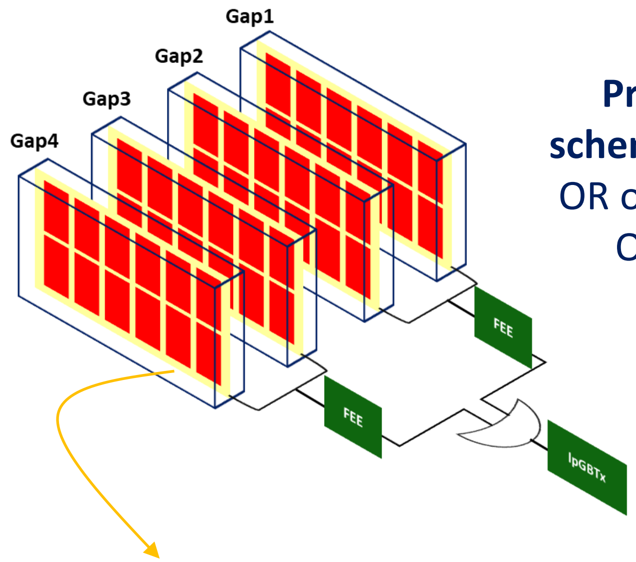

Present readout scheme of a chamber:
OR of 2 gaps, again in OR at FEE level

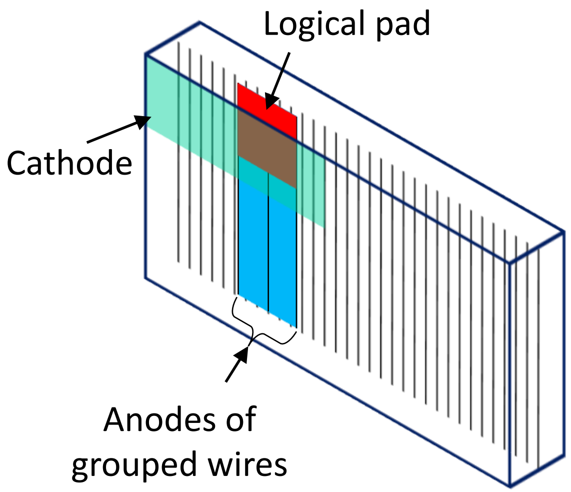

In each gap logical pads are logic AND between grouped wires and strips (or chatode pads)

LHCb muon detector at Run 3

The **muon identification** acts at different levels. The first one is the ***IsMuon*** request such that, given an extrapolated track:

1. The nearest track hit on each station is searched in a *FoI*: area around the extrapolated point on the station

2. The presence of hits on stations is required, according to the momentum:

$p\ [GeV/c]$	The track is a muon:
$p < 3$	never
$3 < p < 6$	M2 & M3
$6 < p < 10$	M2 & M3 & (M4 || M5)
$p > 10$	M2 & M3 & M4 & M5

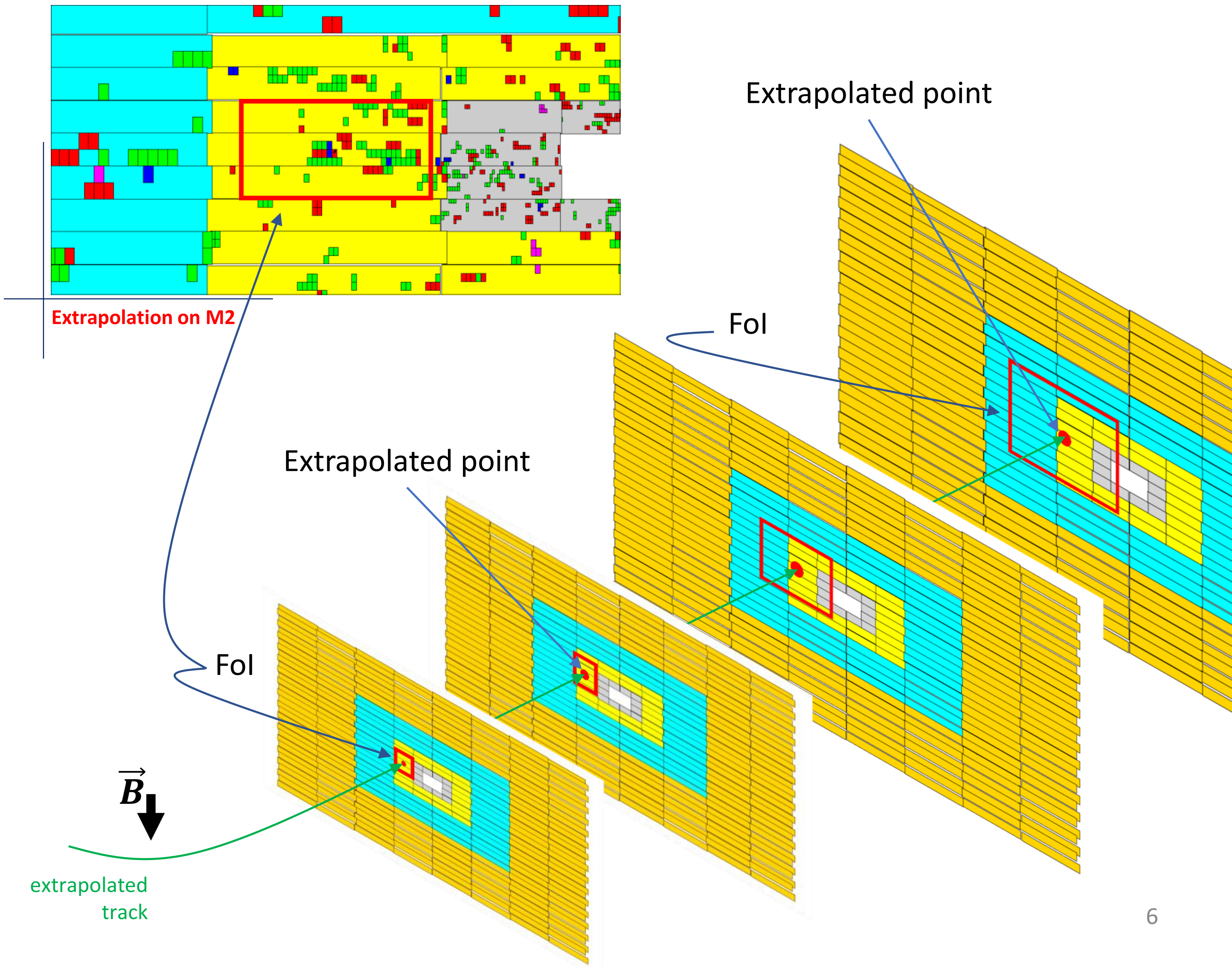

Upgrade II of LHCb apparatus

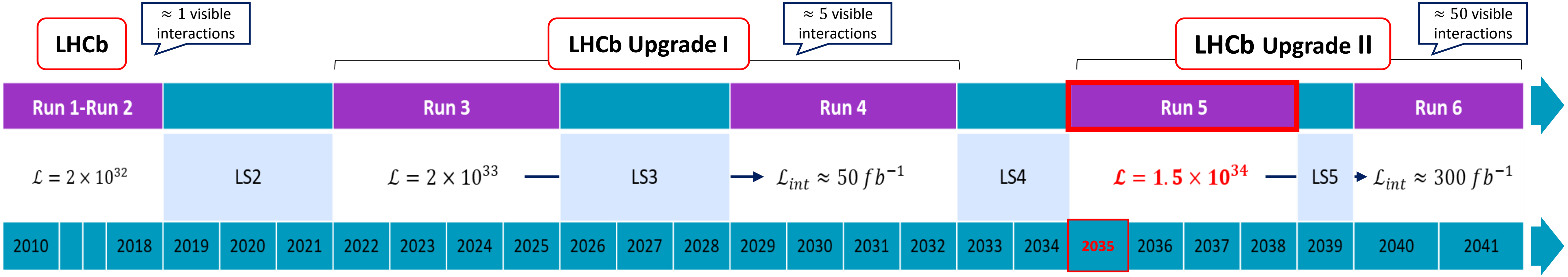

A great opportunity for LHCb:

- Measurements ***precision*** will improve
- More sensibility to ***new physics*** phenomena

Observable	Current LHCb (up to 9 fb^{-1})	Upgrade I (50 fb^{-1})	Upgrade II (300 fb^{-1})
CKM tests			
γ ($B \to DK$, *etc.*)	$4°$	$1°$	$0.35°$
ϕ_s ($B_s^0 \to J/\psi\phi$)	32 mrad	10 mrad	4 mrad
$\lvert V_{ub}\rvert/\lvert V_{cb}\rvert$ ($\Lambda_b^0 \to p\mu^-\overline{\nu}_\mu$, *etc.*)	6%	2%	1%
$a_{\rm sl}^d$ ($B^0 \to D^-\mu^+\nu_\mu$)	36×10^{-4}	5×10^{-4}	2×10^{-4}
$a_{\rm sl}^s$ ($B_s^0 \to D_s^-\mu^+\nu_\mu$)	33×10^{-4}	7×10^{-4}	3×10^{-4}
Charm			
ΔA_{CP} ($D^0 \to K^+K^-, \pi^+\pi^-$)	29×10^{-5}	8×10^{-5}	3.3×10^{-5}
A_Γ ($D^0 \to K^+K^-, \pi^+\pi^-$)	11×10^{-5}	3.2×10^{-5}	1.2×10^{-5}
Δx ($D^0 \to K_S^0\pi^+\pi^-$)	18×10^{-5}	4.1×10^{-5}	1.6×10^{-5}
Rare Decays			
$\mathcal{B}(B^0 \to \mu^+\mu^-)/\mathcal{B}(B_s^0 \to \mu^+\mu^-)$	69%	27%	11%
$S_{\mu\mu}$ ($B_s^0 \to \mu^+\mu^-$)	—	—	0.2
$A_{\rm T}^{(2)}$ ($B^0 \to K^{*0}e^+e^-$)	0.10	0.043	0.016
$A_{\rm T}^{\rm Im}$ ($B^0 \to K^{*0}e^+e^-$)	0.10	0.043	0.016
$\mathcal{A}_{\phi\gamma}^{\Delta\Gamma}(B_s^0 \to \phi\gamma)$	$^{+0.41}_{-0.44}$	0.083	0.033
$S_{\phi\gamma}(B_s^0 \to \phi\gamma)$	0.32	0.062	0.025
$\alpha_\gamma(\Lambda_b^0 \to \Lambda\gamma)$	$^{+0.17}_{-0.29}$	0.097	0.038
Lepton Universality Tests			
R_K ($B^+ \to K^+\ell^+\ell^-$)	0.044	0.017	0.007
R_{K^*} ($B^0 \to K^{*0}\ell^+\ell^-$)	0.12	0.022	0.009
$R(D^*)$ ($B^0 \to D^{*-}\ell^+\nu_\ell$)	0.026	0.005	0.002

LHCB-TDR-023

Upgrade II of muon detector

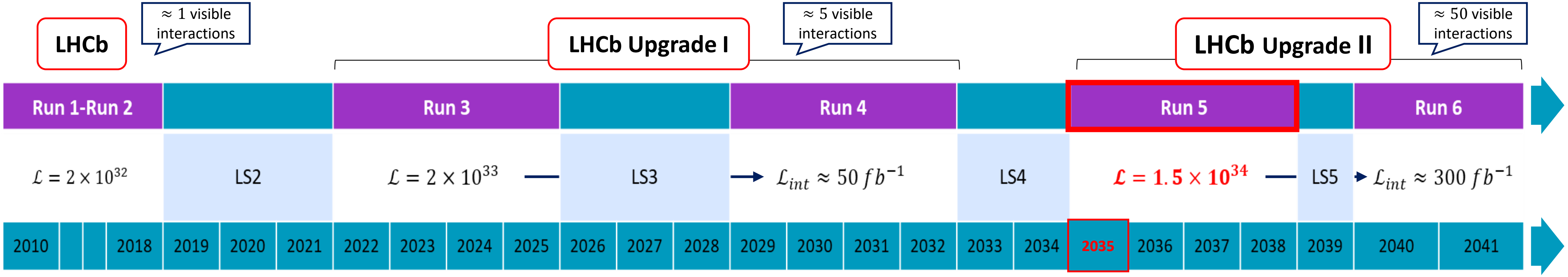

- ❖ Insufficient rate capability of present detector
- ❖ Chambers granularity inadequate for the future high rates
- ❖ High pile-up conditions will cause:
  - inefficiency effects by electronics dead time
  - inefficiency effects of muon mis-identification

during my PhD

- **New readout scheme simulation**
- New detector (**μRWELL**) for inner regions
- **Electronics dead time** effects
- **mis-Identification** effects

Rates estimate at Run 5

At the LHC Run 3 start:
rates measurements of each chambers gap, at seven luminosity configurations

A linear fit for the rates extrapolation at Run 5 luminosity:
$L = 1.5 \times 10^{34}\ cm^{-2} sec^{-1}$

Number of visible *pp* interactions per bunch crossing

$\mu = 1.10$	• $L = 1.05 \times 10^{32}\ cm^{-2}\ s^{-1}$
$\mu = 1.45$	• $L = 1.39 \times 10^{32}\ cm^{-2}\ s^{-1}$
$\mu = 2.29$	• $L = 2.19 \times 10^{32}\ cm^{-2}\ s^{-1}$
$\mu = 2.92$	• $L = 2.79 \times 10^{32}\ cm^{-2}\ s^{-1}$
$\mu = 3.50$	• $L = 3.35 \times 10^{32}\ cm^{-2}\ s^{-1}$
$\mu = 4.05$	• $L = 3.87 \times 10^{32}\ cm^{-2}\ s^{-1}$
$\mu = 4.56$	• $L = 4.36 \times 10^{32}\ cm^{-2}\ s^{-1}$

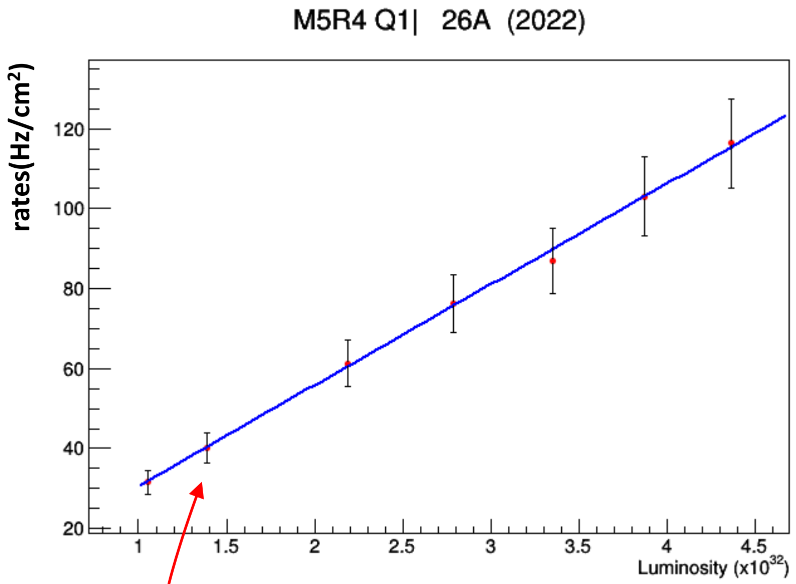

Linear fit to rates/cm² measured at Run 3

Maximum rates (M2) of muon detector design (**Run 1**):

	M2 (kHz/cm²)
R1	37.5
R2	26.5
R3	6.5
R4	1.2

Maximum rates extrapolated at **Run 5**,
in red, reduction in the hypothesis of a **filter** upstream wrt M2

Maximum chamber rate (kHz/cm²)					
	M2	M3	M4	M5	$<\frac{\sigma_R}{R}>$ %
R1	594.0 -> 344.5	274.5	203.5	232.7	10.1%
R2	255.6 -> 79.2	64.2	34.1	39.0	10.2%
R3	53.4 -> 19.2	8.9	6.2	8.9	8.5%
R4	9.9	3.0	1.7	6.8	9.6%

Rates estimate at Run 5

Rates of M2 gaps (Hz/cm^2)

1001	910	1247	1893	2512	1403	1025	1096
917	804	1165	1776	2110	1280	849	1036
1389	784	1307	1931	2106	1299	841	1533
1559	747	1322	2153	2456	1375	811	1743
2347	911	1878	3049	3357	1832	1028	2520
2149	964	2212	3923	4169	2213	1117	2377
3008	1346	3158	6023	6585	3145	1505	3162
2771	1266	3808	8021	9170	3865	1686	2988
3612	2067	5441	12527	13263	5342	2258	3856
6452	2411	6748	17733	20786	7056	2598	3711
4870	3228	10223	29439	32666	10271	3561	5056
4546	3825	12713	47328	53362	12902	4084	4784
6446	5028	17773	66493 120583	148811 77788	19378	5429	6676
5886	5787	23113	99470 217584	255560 107048	23768	6213	6244
8355	7272	31962	147585 321062 538980	508077 340550 170105	32190	7757	8502
7262	7473	34047	187623 594044	573691 205862	35821	7902	7647
9783	7957	39218	193571 496249	549110 217988	37922	8619	9938
6942	6921	30431	143561 341093 558687	546084 344551 152596	30842	7337	7299
7764	6280	25658	103585 209874	248696 114114	25527	6609	8103
5358	4802	17515	65005 122387	135696 73421	17909	5125	5503
5779	4111	14025	49121	48987	14323	4421	5783
3889	3116	9632	30130	31072	9905	3232	4095
4183	2658	8154	19704	21454	8021	2835	4469
5035	1972	4899	12240	13814	5210	2104	3253
3301	1674	2767	9149	9554	4351	1880	3542
2431	1283	2943	5789	6430	2771	1397	2646
2470	1138	2533	4446	4789	2448	1250	2668
1776	891	1725	2909	3107	1702	927	1901
1861	821	1525	2350	2474	1492	876	2060
1200	719	1195	1661	1873	1173	760	1451
1210	864	1387	1765	1854	1316	922	1351
1009	1161	1857	2117	2322	1755	1188	1094

Rates of M2 R1-R2 gaps (Hz/cm^2)

66493	120583	148811	77788
99470	217584	255560	107048
147585	321062 538980	508077 340550	170105
187623	594044	573691	205862
193571	496249	549110	217988
143561	341093 558687	546084 344551	152596
103585	209874	248696	114114
65005	122387	135696	73421

Maximum rates extrapolated at **Run 5**,
in red, reduction in the hypothesis of a **filter** upstream wrt M2

Maximum chamber rate (kHz/cm^2)					$<\frac{\sigma_R}{R}>$ %
	M2	M3	M4	M5	
R1	594.0 -> 344.5	274.5	203.5	232.7	10.1%
R2	255.6 -> 79.2	64.2	34.1	39.0	10.2%
R3	53.4 -> 19.2	8.9	6.2	8.9	8.5%
R4	9.9	3.0	1.7	6.8	9.6%

Background study at Run 5

Fraction of signals of the present readout scheme by
single-gap cases of background particles

Minimum bias
Low threshold:

- Sample of 2600 events at $L = 1.5 \times 10^{34}$ cm^{-2} s^{-1}

97% are **background**: defined as all except muons with $E_{\mu} > 3$ GeV

	M2 (%)	M3 (%)	M4 (%)	M5 (%)
R1	49.5 ± 0.1	56.7 ± 0.1	58.6 ± 0.2	59.4 ± 0.2
R2	49.7 ± 0.1	70.4 ± 0.2	75.0 ± 0.2	76.0 ± 0.2
R1 + R2	49.60 ± 0.05	61.1 ± 0.1	63.6 ± 0.1	64.3 ± 0.1
R3	57.5 ± 0.1	73.0 ± 0.2	76.8 ± 0.3	77.1 ± 0.3
R4	49.7 ± 0.1	66.6 ± 0.3	76.1 ± 0.4	69.0 ± 0.4
R3 + R4	53.6 ± 0.1	70.8 ± 0.2	76.6 ± 0.2	74.0 ± 0.3

Studies for a new readout scheme

Current readout scheme

4-gaps OR-ed
If a charged particle crosses one out of four gaps, a signal is generated

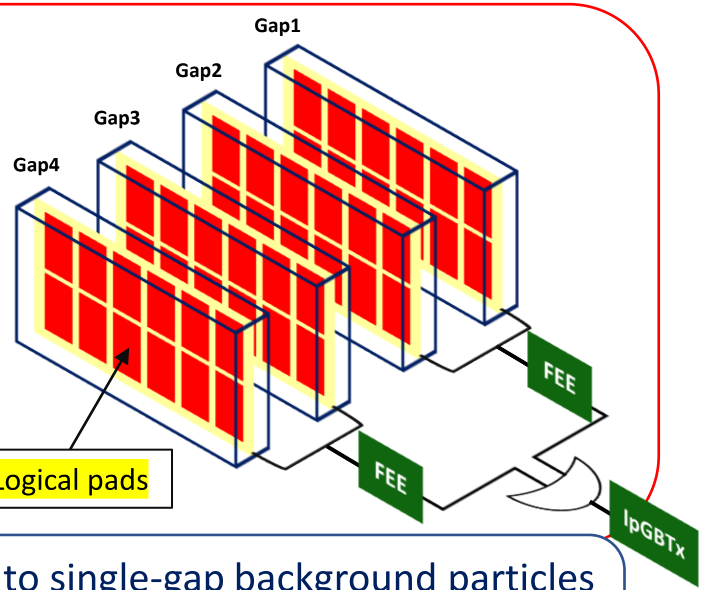

Rates due to single-gap background particles
up to 80%:
The new readout scheme is necessary

Presented at:

PoS LHCP2021 (2021) 192

New readout scheme

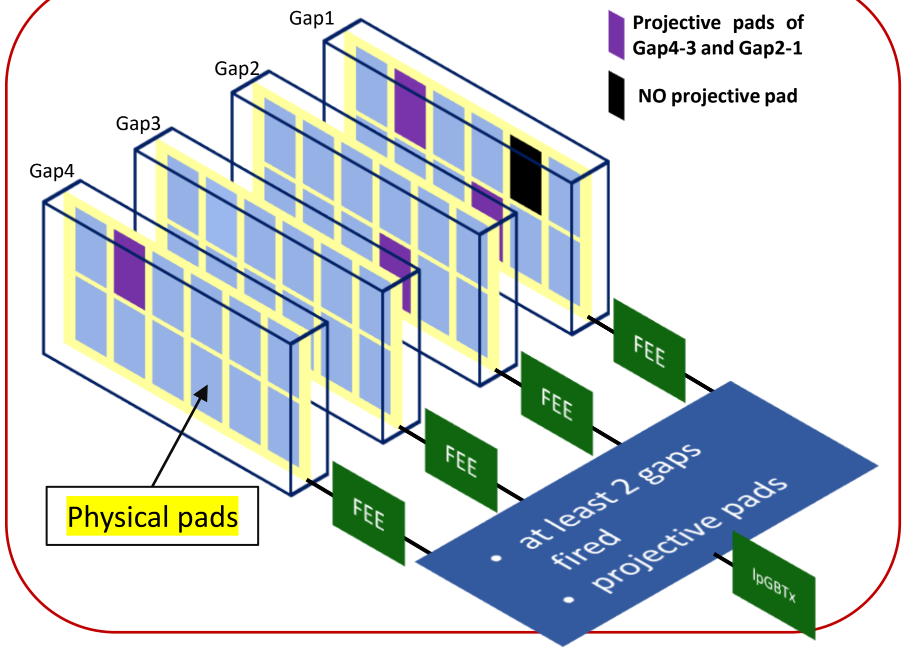

New readout scheme for Upgrade II:

- readout for each gap
- signal in at least 2 gaps out of 4 at the same time
- at least two projective physical pads fired in the corresponding gaps.

Muon Detector simulation

- Physical pads (anodes and cathodes) simulated in chambers at present geometrical configuration (Run 3)

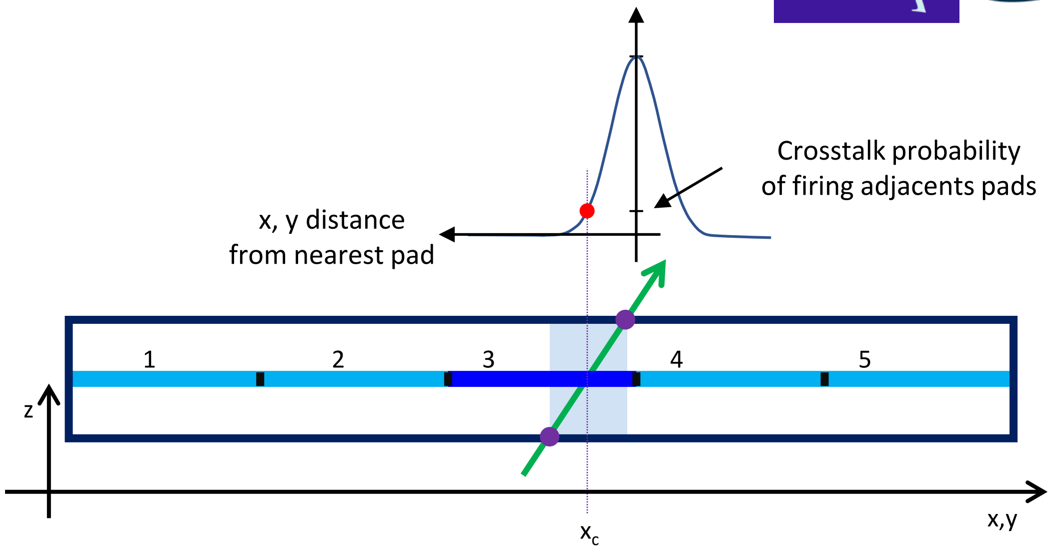

- Electrical and geometrical crosstalk simulated for physical pad firing, at particles chambers crossing

- μ-RWELL in inner regions R1-R2 in the 4-gaps configuration

- Signal generation delay, into 25 ns time window, simulated for present MWPCs and μ-RWELL
  - Efficiency of **85%** for MWPCs and **95%** for μ-RWELLs

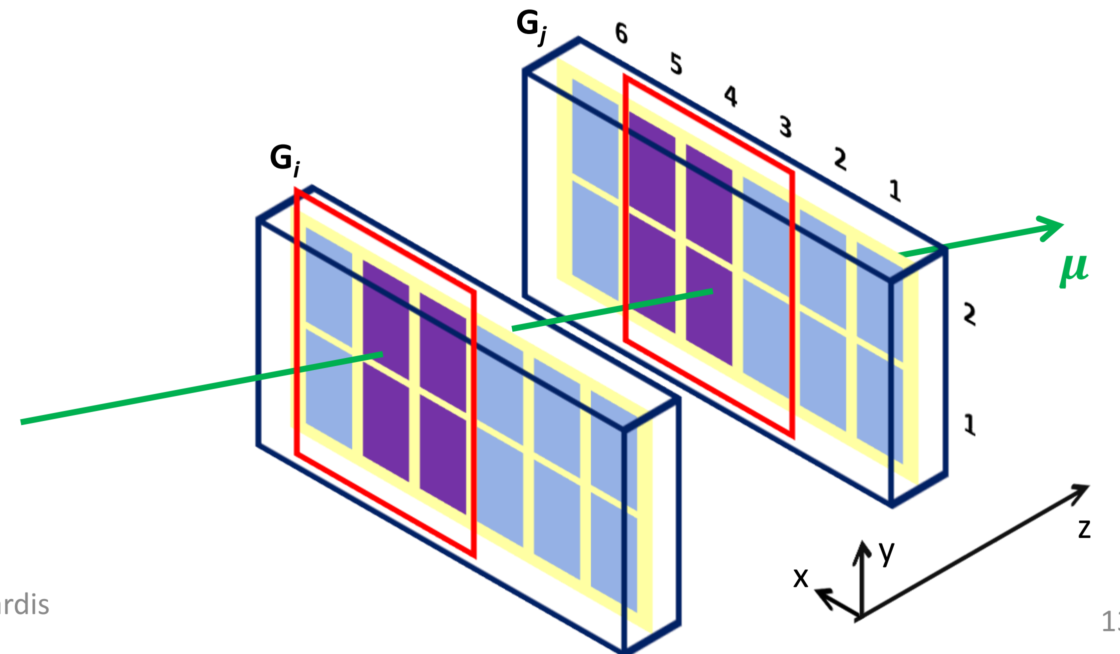

- Projectivity condition, between not only consecutive physical pads, simulated for signal generation
  (not in R4 of M2, M3 and M4 where chambers are fixed at the present OR-ed Bi-gap scheme)

Background reduction with the new readout scheme

μ-RWELL	time-eff= 95%
MWPCs	time-eff= 85%

The new readout scheme has a very significative effect on the background signals removal in the chambers.

A great merit is given by the AND request.

	M2 (%)	M3 (%)	M4 (%)	M5 (%)
R1	66.40 ± 0.07	77.0 ± 0.1	78.20 ± 0.13	78.6 ± 0.1
R2	60.70 ± 0.07	82.10 ± 0.13	86.5 ± 0.2	86.8 ± 0.2
R1–R2 combined	63.50 ± 0.05	78.60 ± 0.08	80.7 ± 0.1	81.0 ± 0.1
R3	64.40 ± 0.09	79.0 ± 0.2	80.8 ± 0.3	81.0 ± 0.3
R4	0.0	0.0	0.0	72.30 ± 0.43
R3–R4 combined	32.10 ± 0.05	50.9 ± 0.1	56.0 ± 0.1	77.70 ± 0.11

What is the effect on signal muons?

Efficiency loss with the new readout scheme

μ-RWELL	time-eff= 95%
MWPCs	time-eff= 85%

CERN/LHCC 2021-012 LHCb TDR 23

$J/\psi \rightarrow \mu^+\mu^-$:

- Sample of 200 000 of $J/\psi \rightarrow \mu^+\mu^-$ candidate.

Inefficiency less than 2%, against the large background reduction up to 80%

The effects of:
-dead time and
-muons mis-identification
are not included

Stations to be crossed for current μ-identification $p\ [GeV/c]$	**overall detector (%)**	inner regions R1-R2 (%)	outer regions R3-R4 (%)
$3 < p < 6$ (M2 & M3)	$\mathbf{1.13 \pm 0.08}$	1.73 ± 0.35	1.09 ± 0.08
$6 < p < 10$ (M2 &M3 & (M4 || M5))	$\mathbf{1.06 \pm 0.06}$	0.70 ± 0.16	1.10 ± 0.07
$p > 10$ (M2 & M3 & M4 & M5)	$\mathbf{2.23 \pm 0.04}$	0.52 ± 0.03	4.04 ± 0.08

μRWELL for Upgrade II

JINST (2019) 289 14 P05014

- Cathode plan
- Derive region
- μRWELL system:
  - Wells to copper clad foil
  - Resistive plate
  - Readout PCB of pad/stip

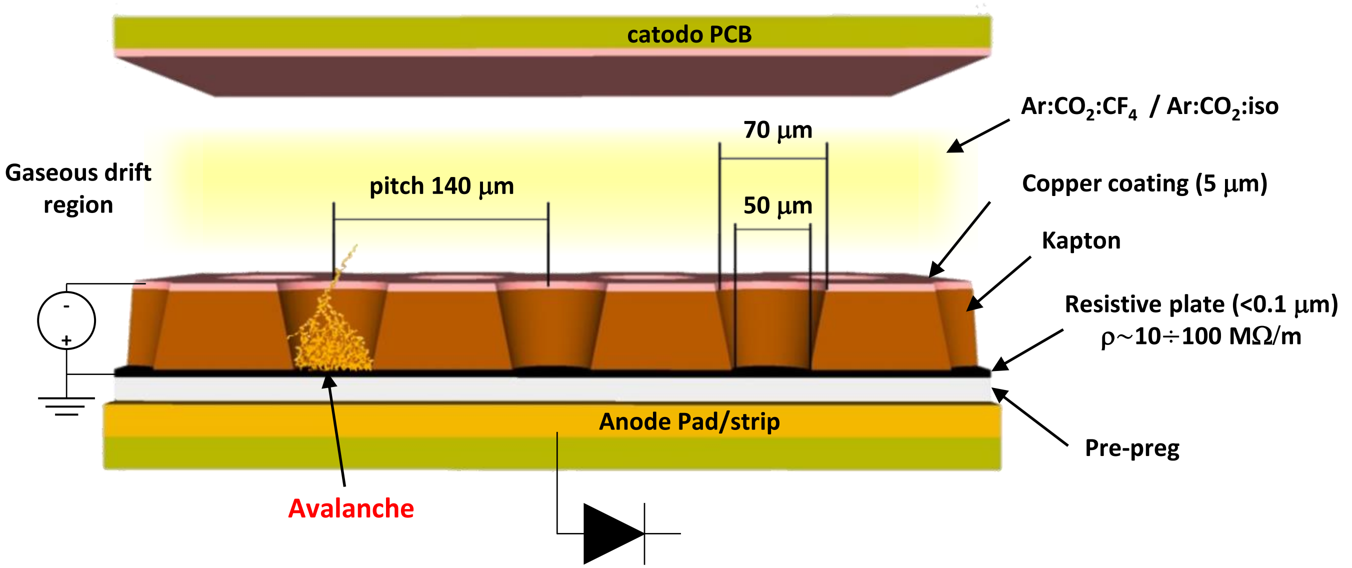

The ionization avalanche in the drift region is amplified in the wells and limited by the resistive plate.

Performances:

- High rate capability (up to 1 MHz/cm^2)
- High granularity, fundamental for the dead time inefficiency reduction

Present pads size [mm]

μ-RWELL pads size [mm]

Reg / Sta	M2	M3	M4	M5
R1	38x31 -> 9x9	41x34 -> 10x10	29x36 -> 11x10	31x39 -> 12x11
R2	76x31 -> 9x18	82x34 -> 10x19	58x73 -> 11x21	62x77 -> 12x22
R3	25x125	27x135	58x145	62x155
R4	50x250	54x270	58x290	62x309

Inefficiency induced by dead time

From Run 5 rates, the inefficiency by the electronics dead time is calculated

- The FEE dead time is assumed conservatively of 100 ns

JINST (2016) 11 P04010

Maximum deadtime inefficiency % HCAL - MWPC	M2	M3	M4	M5
R1	17.14	6.65	7.50	8.66
R2	17.81	4.62	5.69	7.34
R3	7.21	1.72	3.49	5.68
R4	8.24	3.37	2.30	8.55

Maximum deadtime inefficiency % HCAL - µRWELL	M2	M3	M4	M5
R1	1.18	0.48	0.79	0.95
R2	1.22	0.32	0.31	0.41
R3	7.21	1.72	3.49	5.68
R4	8.24	3.37	2.30	8.55

Moving to high-granularity µRWell chambers

Presented at:

IFAE 2023 – Catania

6th Workshop on LHCb upgrade II - Barcellona

A software has been developed to evaluate the dead time effects on decay modes of special interest

SCENARIO		$B_s^0 \to \mu^+\mu^-$ (%)	$D^0 \to \mu^+\mu^-$ (%)	$K_S^0 \to \mu^+\mu^-$ (%)	$B_s^0 \to J/\psi(\mu^+\mu^-)\phi$ (%)
HCAL	MWPC	30.50 ± 0.06	32.10 ± 0.25	25.80 ± 0.35	31.0 ± 0.1
	μ-RWELL	10.30 ± 0.04	9.50 ± 0.16	8.50 ± 0.22	9.60 ± 0.05
SHIELD	MWPC	19.00 ± 0.05	19.40 ± 0.21	14.0 ± 0.3	18.80 ± 0.07
	μ-RWELL	8.60 ± 0.04	7.60 ± 0.14	6.4 ± 0.2	7.80 ± 0.05
w/o M2	MWPC	13.40 ± 0.04	17.2 ± 0.2	10.70 ± 0.24	16.4 ± 0.1
	μ-RWELL	6.00 ± 0.03	5.30 ± 0.12	3.20 ± 0.14	5.30 ± 0.04

The muon mis-IDentification

The **muon identification** acts at different levels:

2. For each IsMuon track candidate, the χ^2_{corr} is calculated, from distances between the extrapolated points and hits on stations
   JINST 15 (2020) T12005

3. Cut on χ^2_{corr} is applied

<u>False muon hits</u> can be identified on stations at very crowded environment.

Development of a software to simulate the full hits generation at Run 5, in 25 ns time window :

- New *FoI* definitions
- Different χ^2_{corr} cut

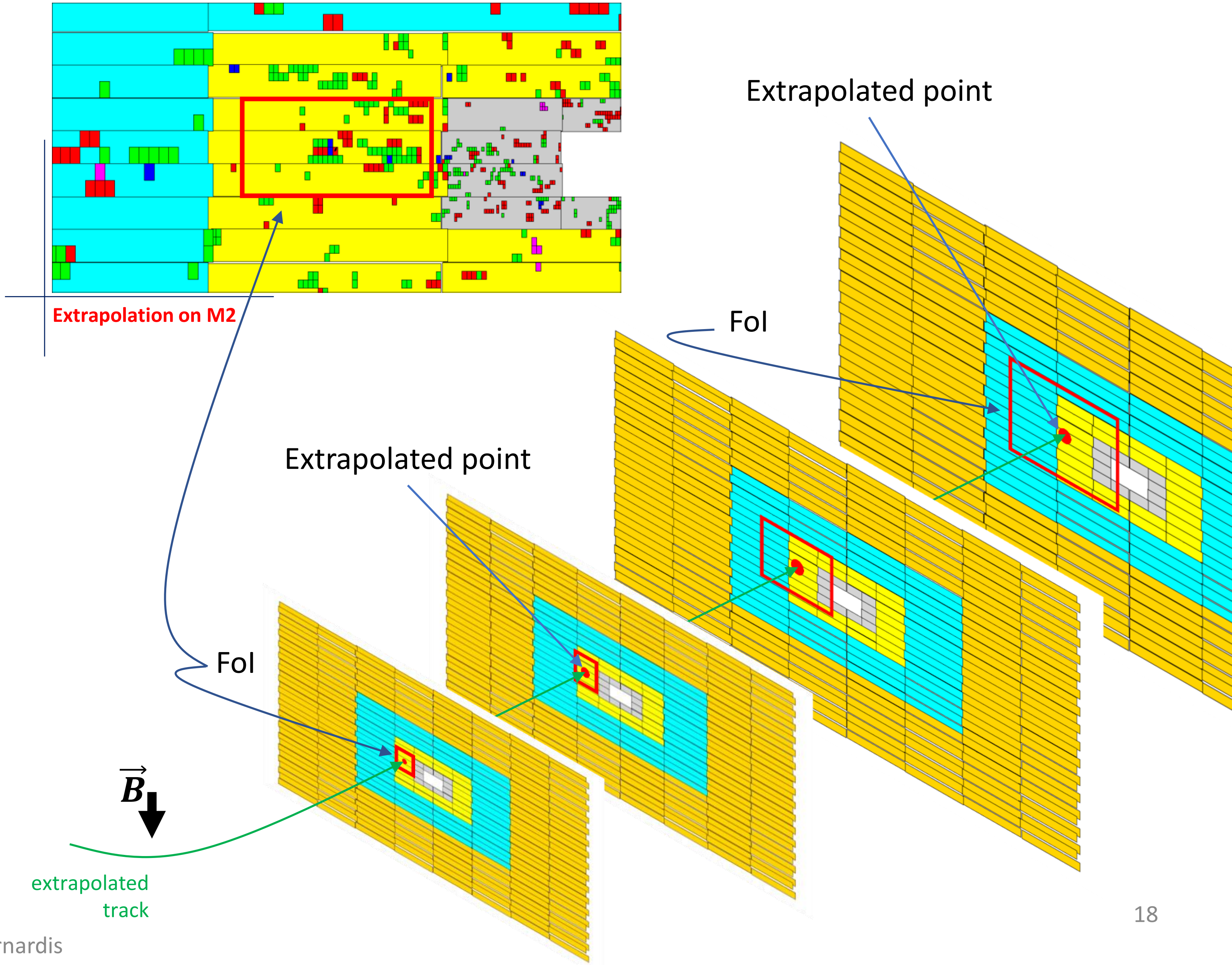

Outline

- Studies on the design of the LHCb muon detector at high luminosity
    - Rate estimate
    - Proposal of a new readout scheme
    - Dead time and muon ID

- Search for the rare decay mode $D_{s1}(2460)^{+} \rightarrow {D_s}^{+}\mu^{+}\mu^{-}$
    - Optimisation of the D_s selection
    - $D_s^{+}\mu^{+}\mu^{-}$ selection
    - Observation of new decay modes

The puzzle of the $D_{s1}(2460)$ meson

Theoretical predictions

- Broad $c\bar{s}$ meson state
- Massive enough that dominant strong decays would have been isospin-conserving in D^*K final states.

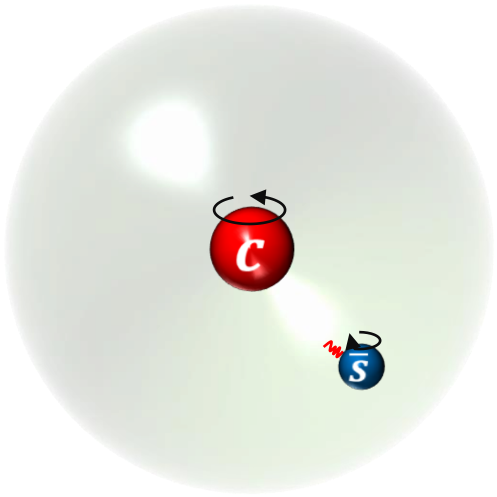

Phys. Rev. Lett. 66 (1991) 1130
Phys. Rev. D 12 (1975) 147

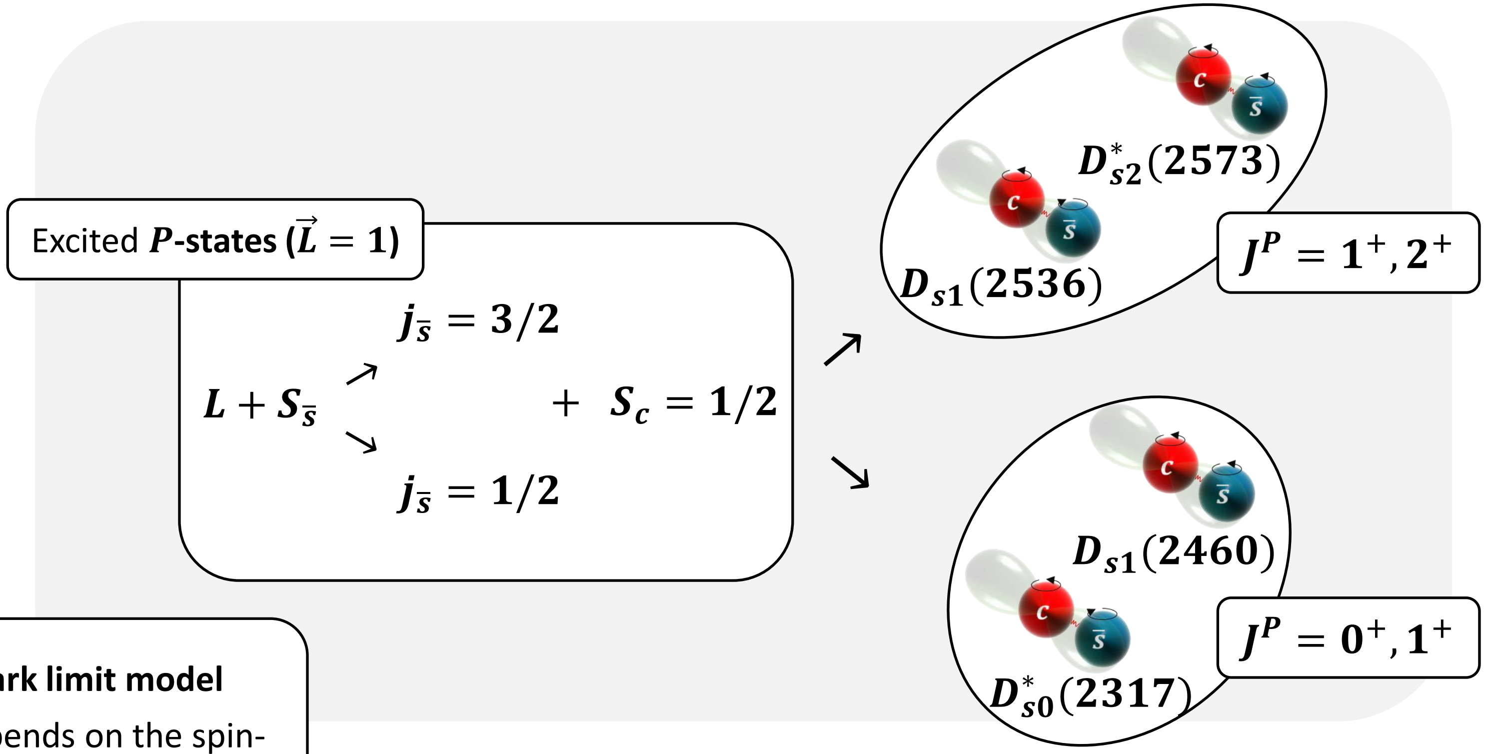

In the heavy quark limit model

Bounding force depends on the spin-orbit coupling only of the light $\bar{s}$ quark

The puzzle of the $D_{s1}(2460)$ meson

Surprising observation:
$\boldsymbol{D_{s1}(2460)^+ \to D_s^{*+}\pi^0}$
***CLEO* (2003)**

- mass smaller ($\approx$ 150 MeV) than all theoretical predictions
- observed in the isospin-violating $D_s^*\pi^0$ channel
- narrow state

$\boldsymbol{D_{s1}(2460)^+}$

decay modes	
$D_s^{*+}\pi^0$	$(48 \pm 11)\%$
$D_s^+\gamma$	$(18 \pm 4)\%$
$D_s^+\pi^+\pi^-$	$(4.3 \pm 1.3)\%$
TOT	$(\mathbf{70 \pm 16})\%$

In a c$\bar{s}$ scenario: isospin-violating decay is suppressed.

For the $\boldsymbol{D_{s1}(2460)}$: isospin-violating decay $D_s^*\pi^0$ is much frequent, suggesting a 4-quarks system (c$\bar{s}u\bar{u}$ or c$\bar{s}d\bar{d}$)

Dalitz decays

- $\pi^0 \to \gamma\gamma^* \to \gamma e^+e^-$ decay process predicted by R.H. Dalitz. The virtual photon directly produces an electron-positron pair.

(nowadays)

- Any decay process with two leptons in the final state, produced by a virtual photon.

Optimisation of the D_s^+ selection

BEFORE

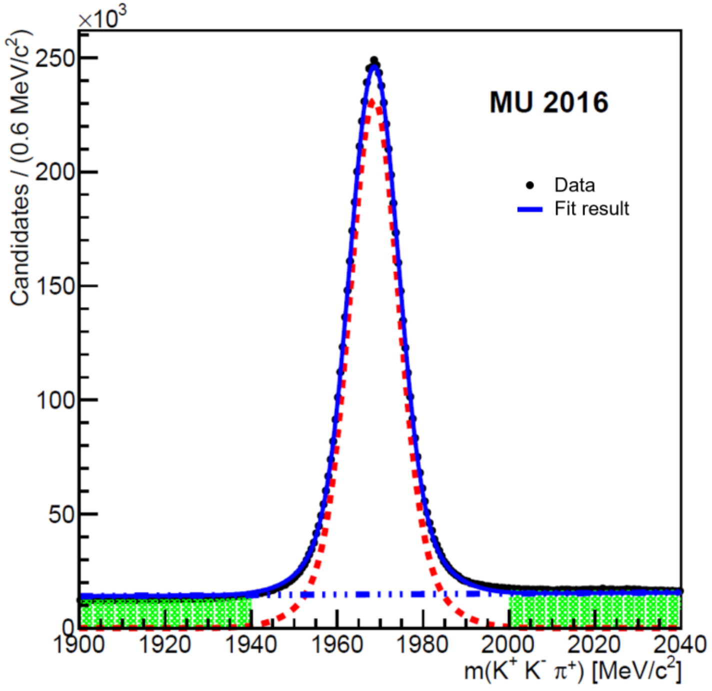

sFit to the $K^+K^-\pi^+$ mass spectrum

BDT multivariate analysis to classify:
-**signal** candidates (s-weighted D_s^+ distribution)
and
-**background** candidates (sidebands).

AFTER

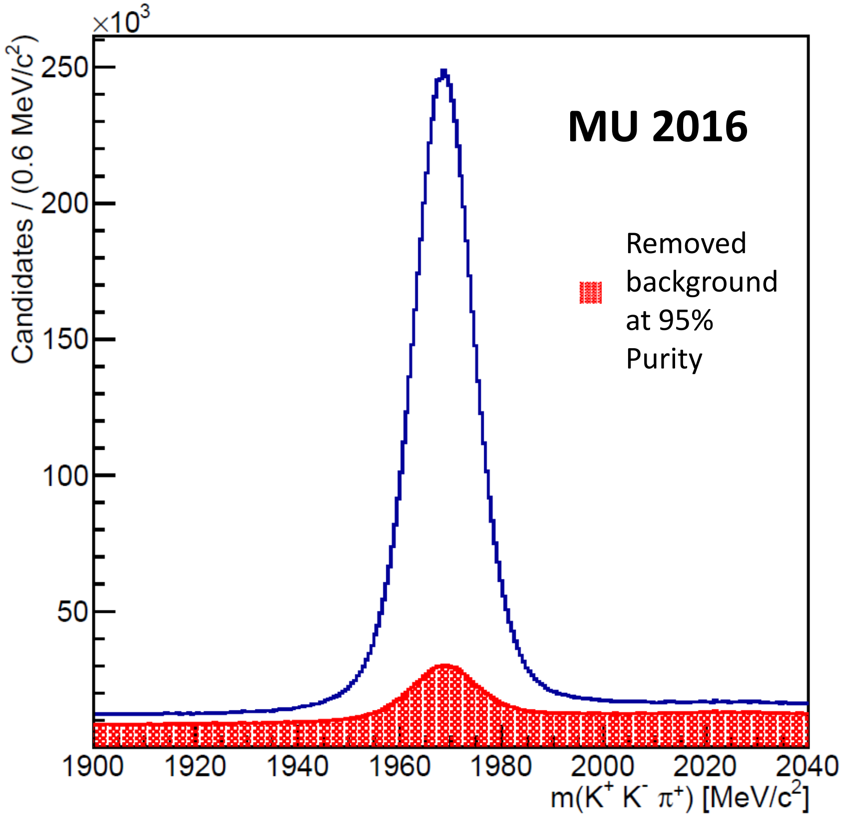

$D_s^+\mu^+\mu^-$ selection

RUN 2
(2015-2018)
$6\ fb^{-1}$

$D_{s1}(2460)^+ \rightarrow D_s^+\mu^+\mu^- + c.c.$

$D_{s1}(2460)^+ \rightarrow D_s^+\mu^+\mu^+ + c.c$

$D_{s1}(2460)^+ \rightarrow D_s^+\mu^-\mu^- + c.c.$

- **D_s candidates:**
  multivariate selection application

- **$D_{s1}(2460)$ candidates:**

  -BDT and BDTG algorithms for signal and background events classifications.

  - **MC samples as signal input**
    (½ for training and ½ for testing)

  - **Wrong Signs sample**
    as a proxy of **combinatorial background**
    (½ for training and ½ for testing)

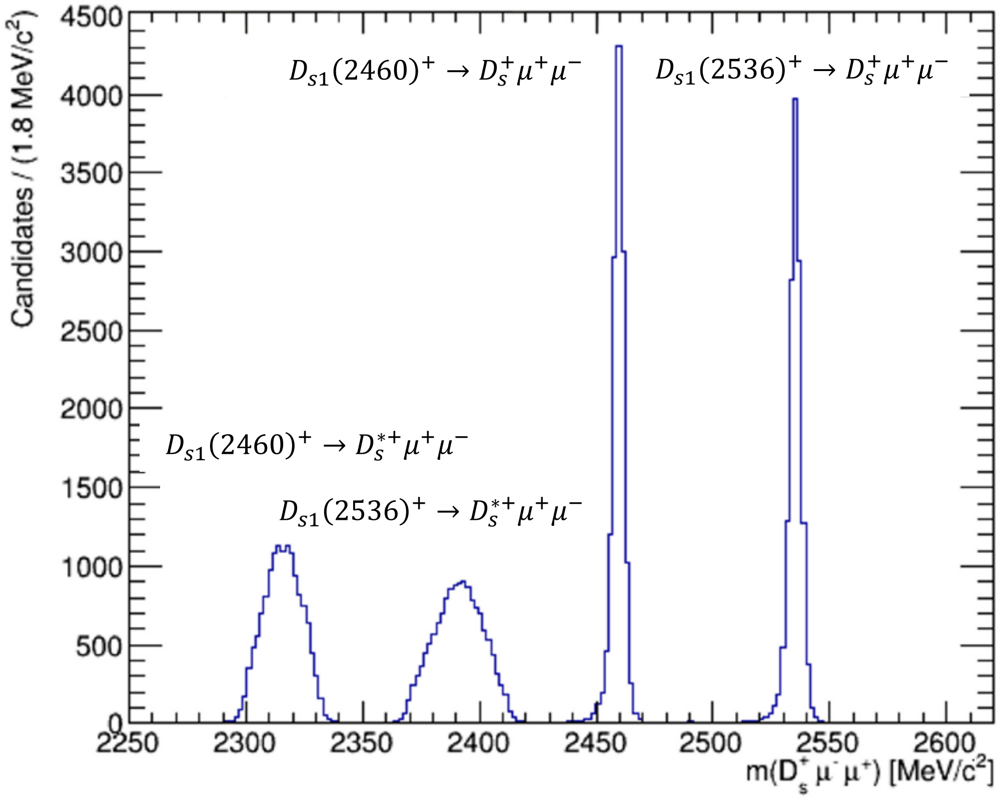

Presented at:

EPJ Web Conf. 270 (2022) 00013

LHCb Italia 2022 Collaboration Meeting

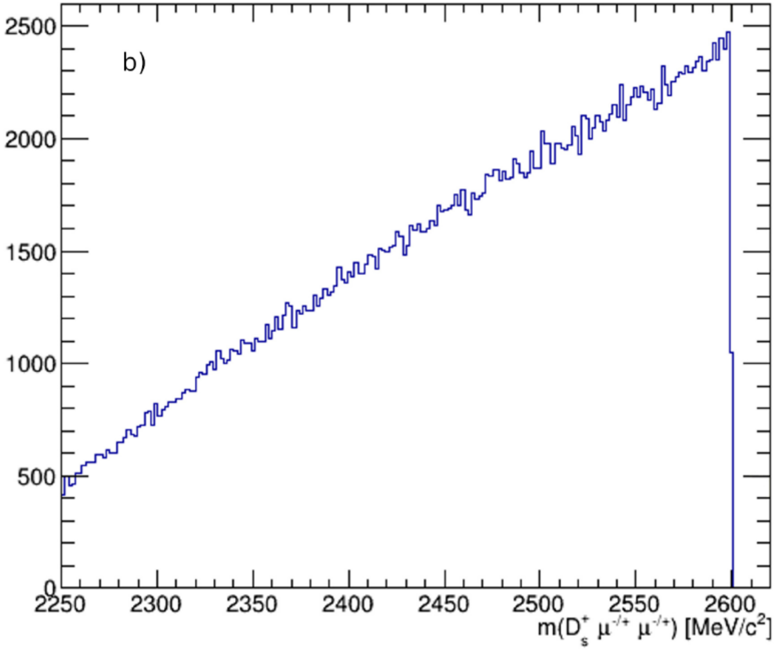

Fit result:

RUN 2
(2015-2018)
$6\ fb^{-1}$

Fit model
(PDF_{total})

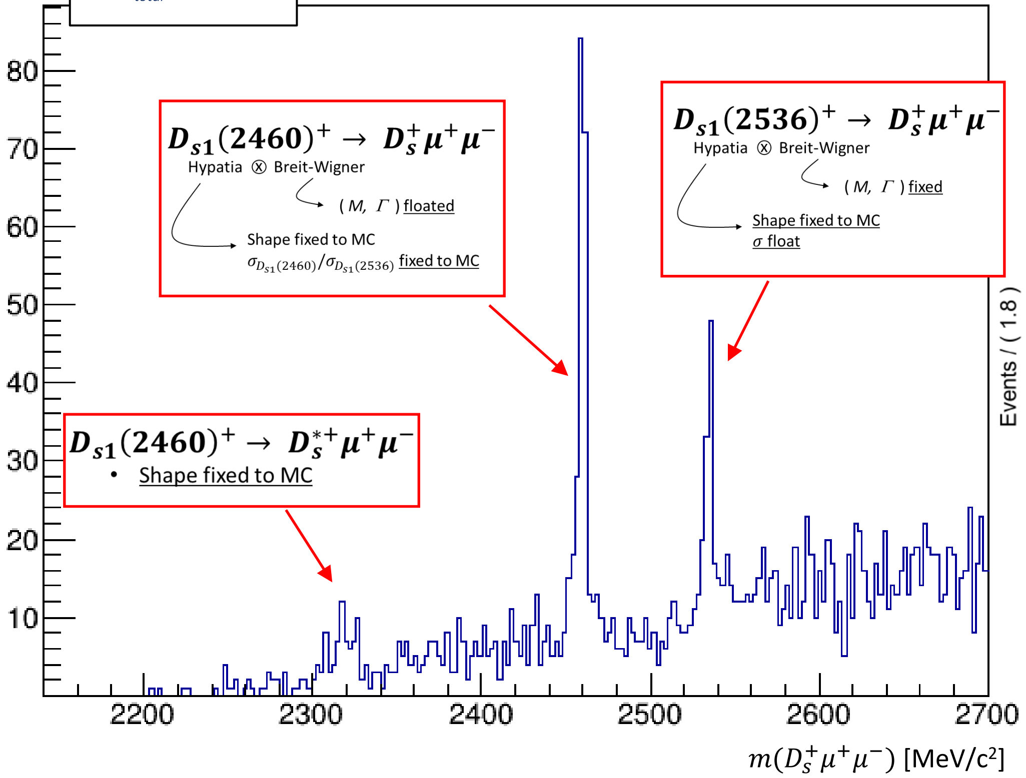

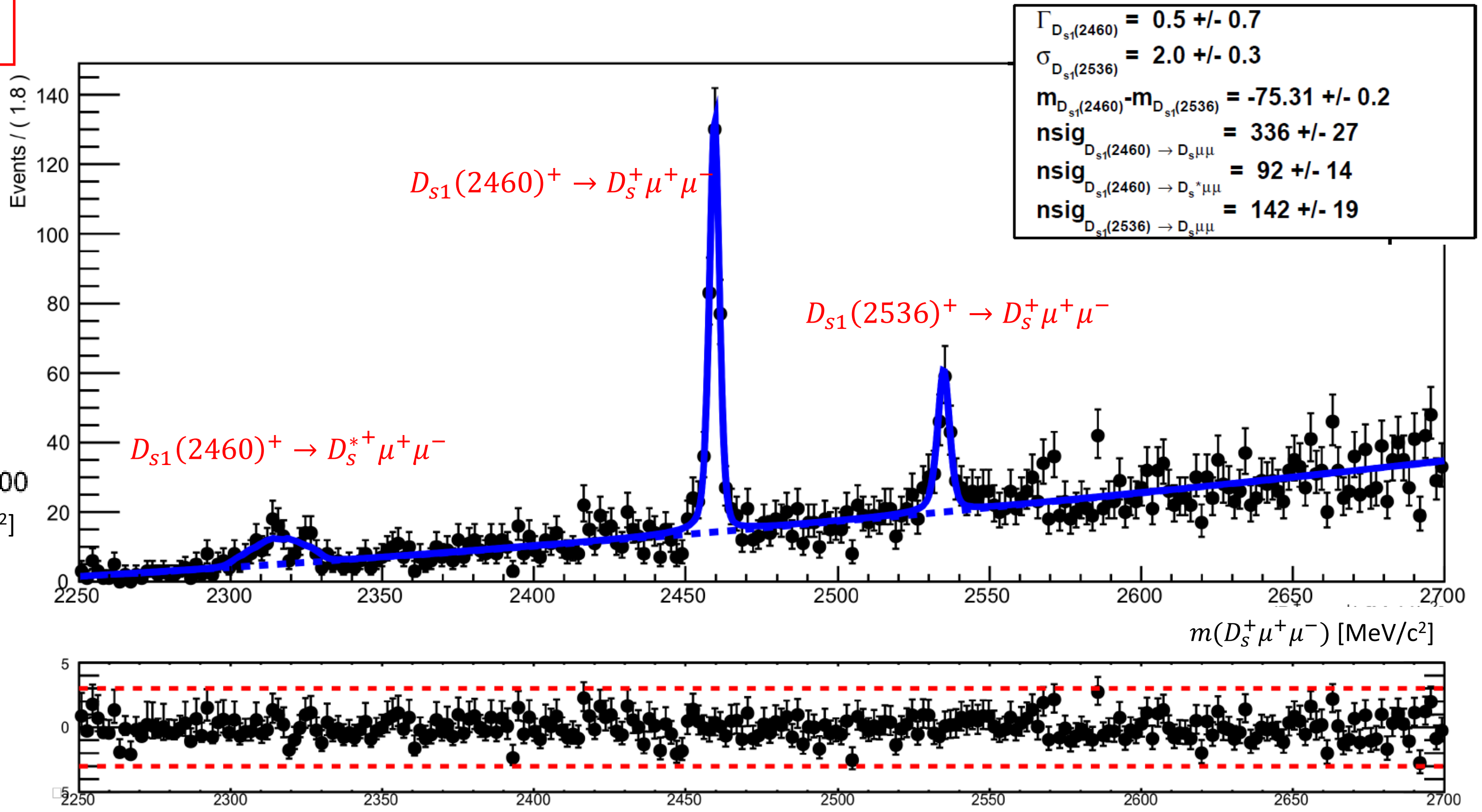

New observations:

- $m_{D_{s1}(2460)} = 2459.9 \pm 0.2 \ \ \mathrm{MeV/c^2}$
- $\Gamma_{D_{s1}(2460)} = \ 0.5 \pm 0.7 \ \ \mathrm{MeV/c^2}$

upper limit evaluated at 95% CL:

$\Gamma_{D_{s1}(2460)} < \ 1.77$ MeV/c2

⇔

$D_{s1}(2460)^{\pm}$	**MASS**	$2459.5 \pm 0.6\ \mathrm{MeV/c^2}$
$D_{s1}(2460)^{\pm}$	**WIDTH**	$< 3.5 \ \ \mathrm{MeV/c^2}$

PDG

New observations:

- $m_{D_{s1}(2460)} = 2459.9 \pm 0.2 \ \ \mathrm{MeV/c^2}$
- $\Gamma_{D_{s1}(2460)} = \ 0.5 \pm 0.7 \ \ \ \mathrm{MeV/c^2}$

upper limit evaluated at 95% CL:
$\Gamma_{D_{s1}(2460)} < \ 1.77$ MeV/c2

$D_{s1}(2460)^{\pm}$	**MASS**	$2459.5 \pm 0.6 \ \mathrm{MeV/c^2}$
$D_{s1}(2460)^{\pm}$	**WIDTH**	$< 3.5 \ \ \mathrm{MeV/c^2}$

PDG

$$\frac{\mathfrak{B}(D_{s1}(2460) \to D_s^* \mu^+\mu^-)}{\mathfrak{B}(D_{s1}(2460) \to D_s\mu^+\mu^-)} = \mathrm{BR\_2460} \cdot \frac{\epsilon_1}{\epsilon_2} = 0.48 \pm 0.10$$

$D_{s1}(2460) \to D_s^* \mu^+\mu^-$

peak significance : $n_\sigma = 7.7\sigma$

NEW DECAY OBSERVATION

New observations:

- $m_{D_{s1}(2460)} = 2459.9 \pm 0.2 \ \ \mathrm{MeV/c^2}$
- $\Gamma_{D_{s1}(2460)} = \ 0.5 \pm 0.7 \ \ \ \mathrm{MeV/c^2}$

upper limit evaluated at 95% CL:
$\Gamma_{D_{s1}(2460)} < \ 1.77$ MeV/c2

$D_{s1}(2460)^{\pm}$ **MASS**	$2459.5 \pm 0.6\ \mathrm{MeV/c^2}$	
$D_{s1}(2460)^{\pm}$ **WIDTH**	$< 3.5 \ \ \ \mathrm{MeV/c^2}$	**PDG**

$$\frac{\mathfrak{B}(D_{s1}(2460) \to D_s^* \mu^+\mu^-)}{\mathfrak{B}(D_{s1}(2460) \to D_s\mu^+\mu^-)} = \mathrm{BR\_2460} \cdot \frac{\epsilon_1}{\epsilon_2} = 0.48 \pm 0.10$$

$D_{s1}(2460) \to D_s^* \mu^+\mu^-$

peak significance : $n_\sigma = 7.7\sigma$

NEW DECAY OBSERVATION

First observation of the decay: $D_{s1}(2536) \to D_s^+ \mu^+\mu^-$

Unexpected observation,
given that the corresponding radiative decay is not seen

Is it a Dalitz decay?

Study of the $\mu^+\mu^-$ spectrum:

$D_{s1}(2460)^+ \to D_s^{*+}\mu^+\mu^-$

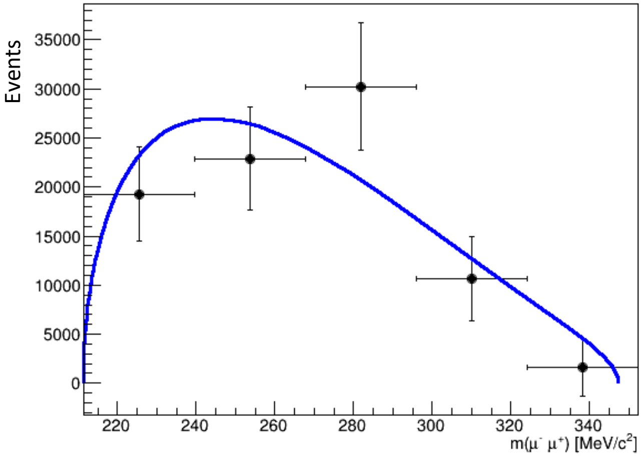

$D_{s1}(2460)^+ \to D_s^{+}\mu^+\mu^-$

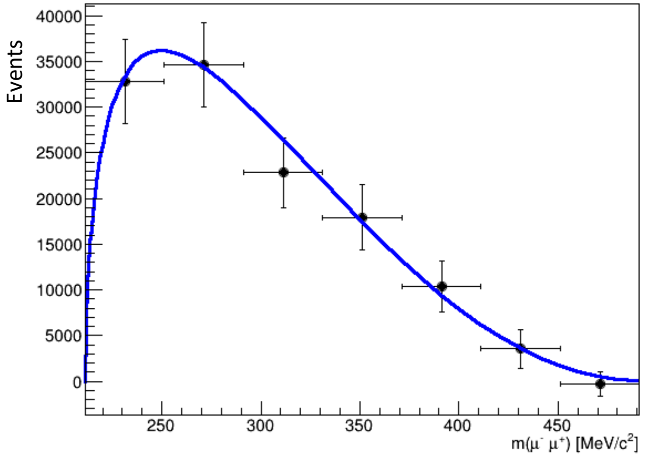

$D_{s1}(2536)^+ \to D_s^{+}\mu^+\mu^-$

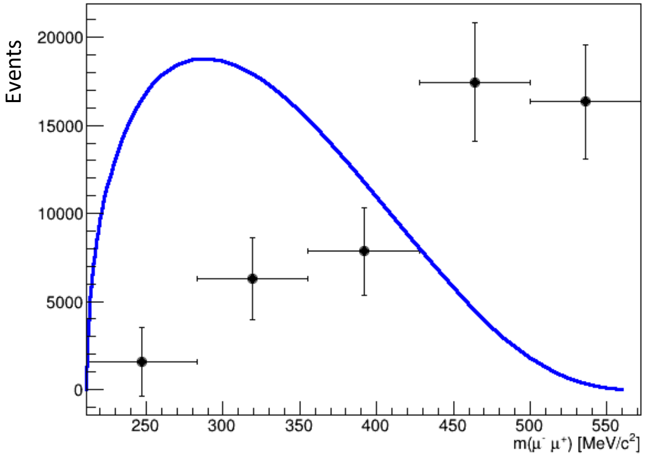

Fits using models built for the Dalitz processes in the QCD framework
[Phys. Rev. D 108, 074027 - 2023]

A virtual photon couples to a c and $\bar{s}$ quark. The latter through an intermediate ϕ meson, according to the Vector Meson Dominance model.

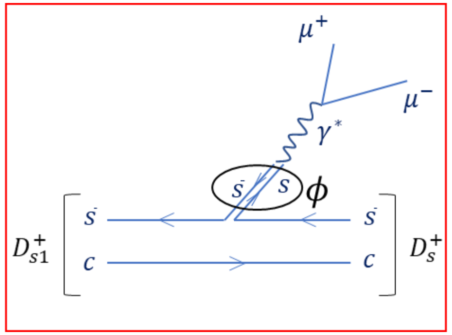

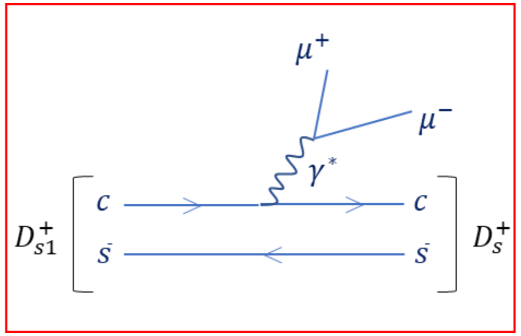

Dalitz nature can be supported for decays:

- $\boldsymbol{D_{s1}(2460)^+ \to D_s^{+*}\mu^+\mu^-}$
- $\boldsymbol{D_{s1}(2460)^+ \to D_s^{+}\mu^+\mu^-}$

Dalitz nature is disfavoured for decay:

- $D_{s1}(2536)^+ \to D_s^{+}\mu^+\mu^-$

Summary

- Studies for the muon detector at high luminosity
  - New readout scheme and μ-RWELL in the inner regions
  - Large background hits reduction up to 80%
  - Inefficiency induced by dead time under study. New scenarios proposed
  - Preliminary results on μ mis-ID studies pave the way to deeper investigations and new ideas

- Search for the rare decay mode $D_{s1}(2460)^+ \rightarrow {D_s}^+\mu^+\mu^-$
  - Precise measurements of $m_{D_{s1}(2460)}$ and $\Gamma_{D_{s1}(2460)}$
  - New observation of the $D_{s1}(2460)^+ \rightarrow D_s^{*+}\mu^+\mu^-$ decay
  - Precise measurement of $\mathfrak{B}(D_{s1}(2460) \rightarrow D_s^* \mu^+\mu^-)/\mathfrak{B}(D_{s1}(2460) \rightarrow D_s\mu^+\mu^-)$
  - New observation of the $D_{s1}(2536)^+ \rightarrow D_s^+\mu^+\mu^-$ decay

Thank you
for your attention

BACKUP

Background study at Run 5

Minimum bias
Low threshold:

- Sample of 2600 events at $L = 1.5 \times 10^{34}$ **cm^{-2} s^{-1}**

≈**800** charged particles cross the detector at each bunch crossing:

$e^{\pm}$	69%	
$\pi^{\pm}$	12%	
$p^{\pm}$	12%	
$\mu^{\pm}$	6%	(all)
	3%	(bckg)
$K^{\pm}$	0.6%	
$nucl$	0.4%	

Background particles distribution in regions:

R1:	37%	66%
R2:	29%	
R3:	18%	34%
R4:	16%	

Electrons:

R1:	36 %
R2:	28 %
R3:	18 %
R4:	18 %

Pions:

R1:	48 %
R2:	32 %
R3:	13 %
R4:	7 %

Protons:

R1:	41 %
R2:	32 %
R3:	17 %
R4:	10 %

Muons ($E_{\mu} < 3$ GeV) **:**

R1:	18 %
R2:	23 %
R3:	21 %
R4:	38 %

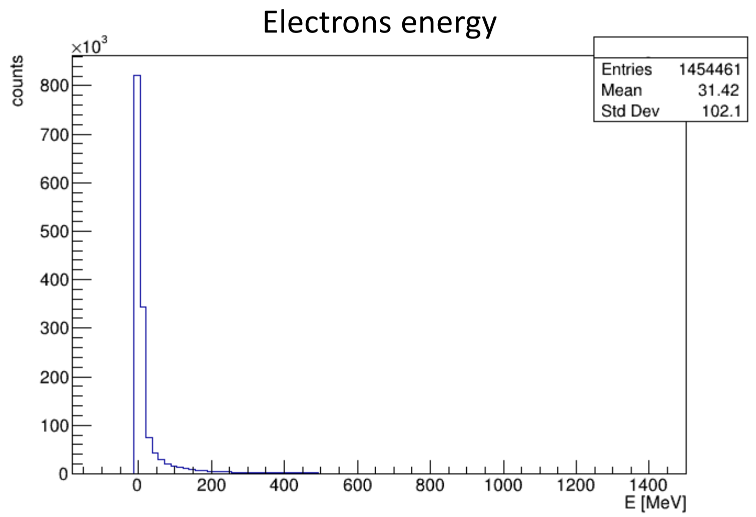

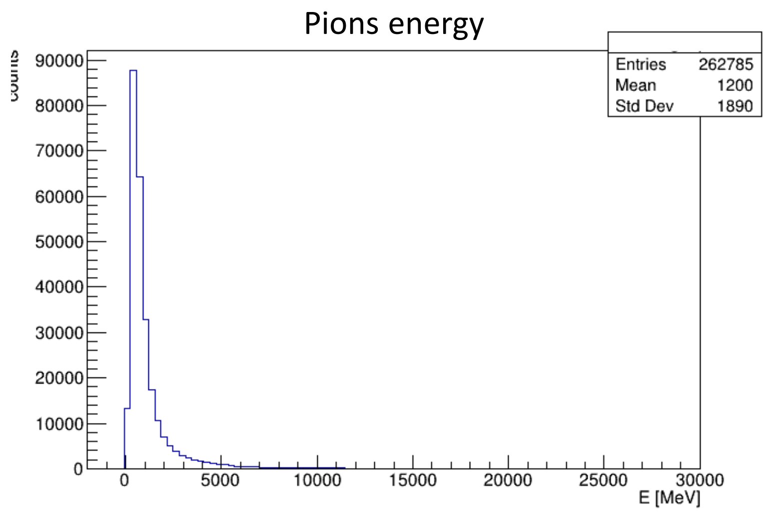

Francesco Debernardis

Projectivity and time inefficiency improvements

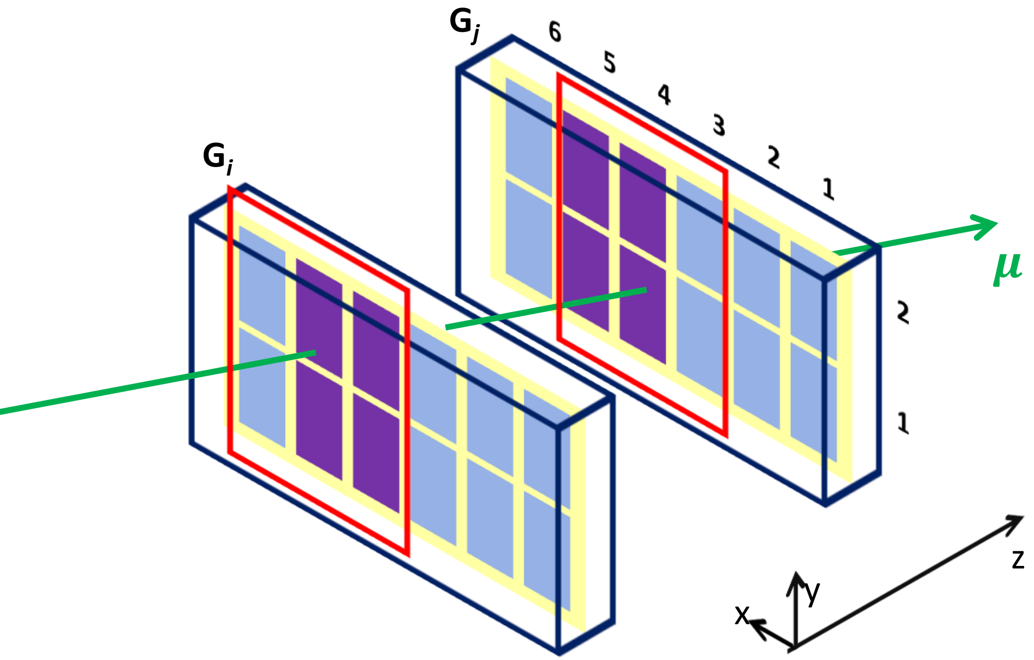

A chamber is fired if at least one couple of **not only consecutive** gaps, have at least two fired projective pads.

Pads that could be fired (P=1) or not fired (P=0), in gaps G_i and G_j.
Of them, violet pads in a gap are projective with respect to those in the other gap.

MWPCs

As preliminary evaluation, **Single gap Time Efficiency (SgTE) equal to**: **85%**

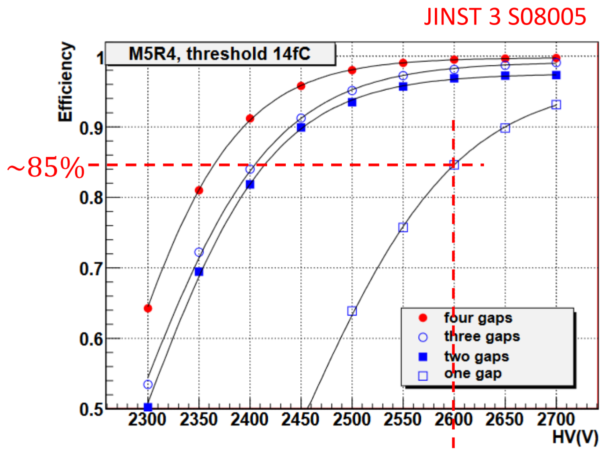

μRWELL

As preliminary evaluation, **Single gap Time Efficiency (SgTE) equal to**: **95%**

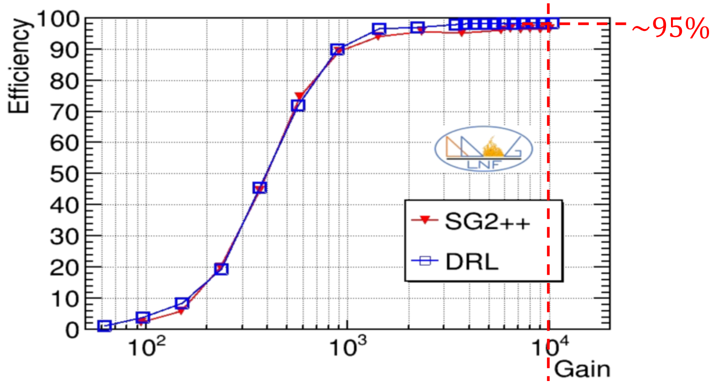

Muon Detector simulation

- Physical pads (anodes and cathodes) simulated in chambers at present geometrical configuration (Run 3)

- Electrical and geometrical crosstalk simulated for physical pad firing, at particles chambers crossing

- μ-RWELL in inner regions R1-R2 in the 4-gaps configuration

- Signal generation delay, into 25 ns time window, simulated for present MWPCs and μ-RWELL
  - Efficiency of **85%** for MWPCs and **95%** for μ-RWELLs

- Projectivity condition, between not only consecutive physical pads, simulated for signal generation
  (not in R4 of M2, M3 and M4 where chambers are fixed at the present OR-ed Bi-gap scheme)

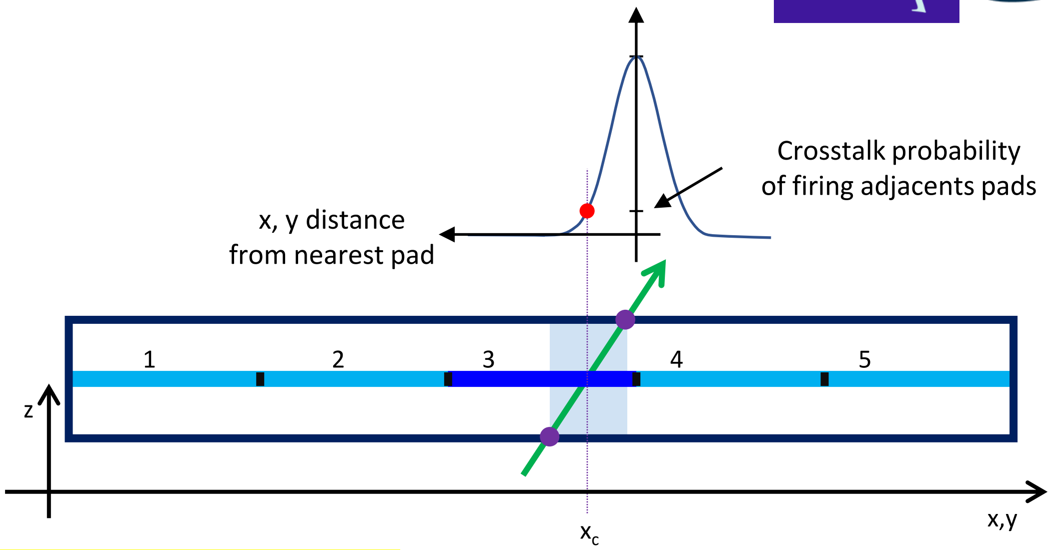

LHCB-MUON 2001-120 V2.0
CERN-LHCb-2001-150
CERN-LHCb-2003-167
CERN-LHCb-2003-001

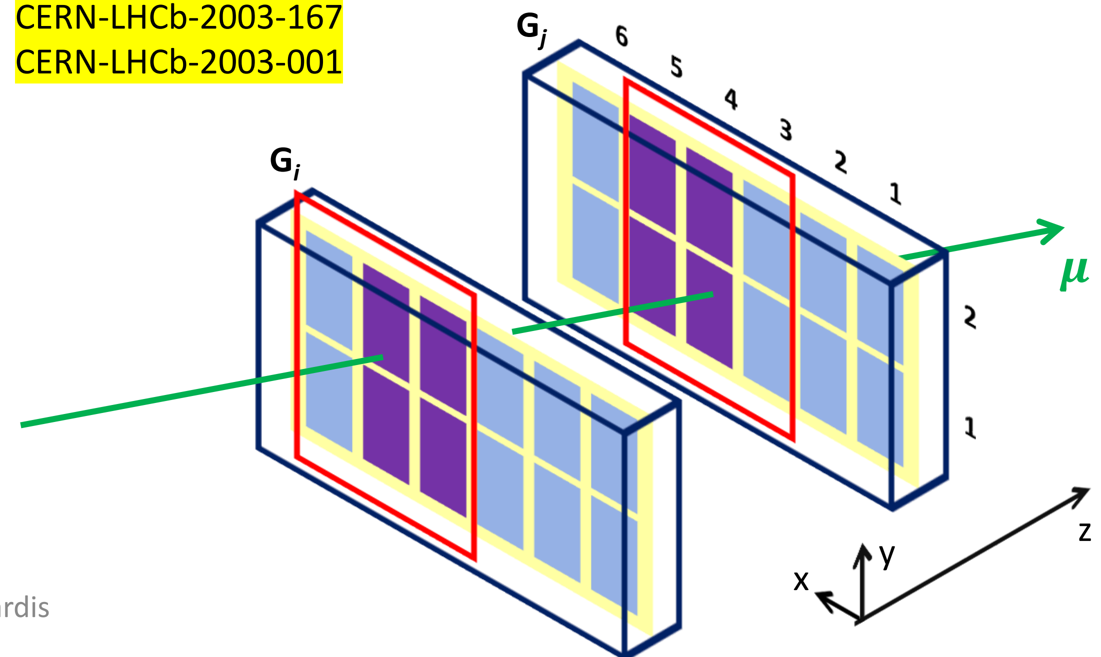

Le μRWELL

JINST (2019) 289 14 P05014

Un rivelatore μRWELL è un MicroPattern Gas Detector (MPGD) che consiste principalmente dei seguenti elementi:

- Piano catodico
- Regione di deriva
- Scheda μRWELL, compattata con:
  - foglio di kapton forato e rivestito in rame
  - Strato resistivo
  - PCB di readout con segmentazione a pad/stip

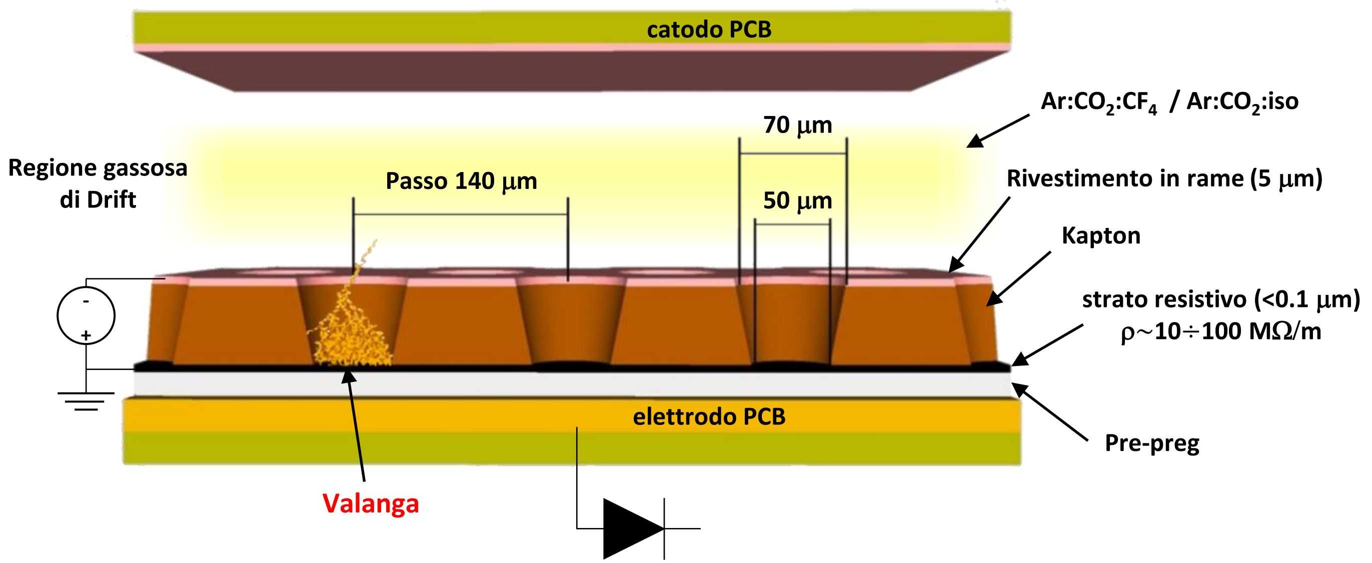

La ionizzazione a valanga, generata nella regione di drift, è amplificata nei fori ed è controllata grazie allo strato resistivo.

La perdita di efficienza ad alti rates (Run 5) è risolta con una fitta rete di elettrodi di messa a terra che evacuano rapidamente le valanghe.

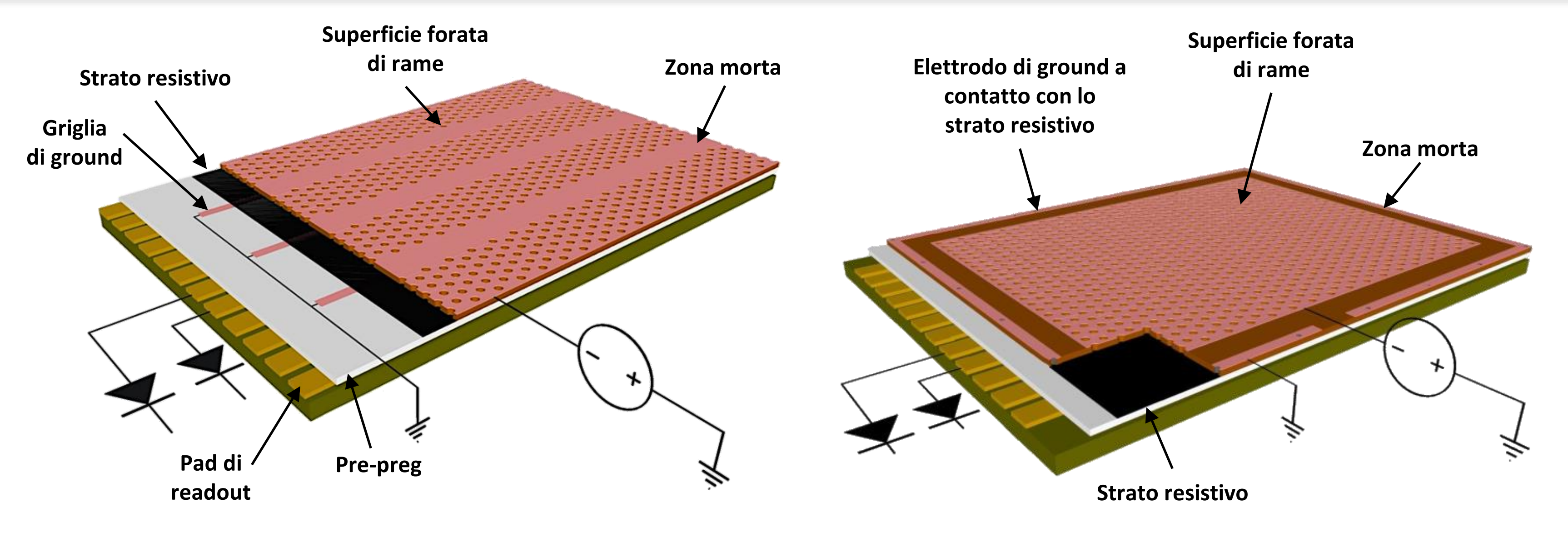

Le μRWELL

JINST (2019) 289 14 P05014

Prestazioni:

- elevata rate capability (**fino a 1 MHz**)
- elevata efficienza in risposta temporale
  $\epsilon = 96\%$ con miscela $Ar:CO_2:CF_4$ = 45:15:40
  in fase di studio con miscela $Ar:CO_2$:iso = 68:30:02
- Dimensioni fino a 1.2x0.5 m
- **elevata granularità**
  che ha un effetto molto significativo
  sull'inefficienza da tempo morto (dopo ->)

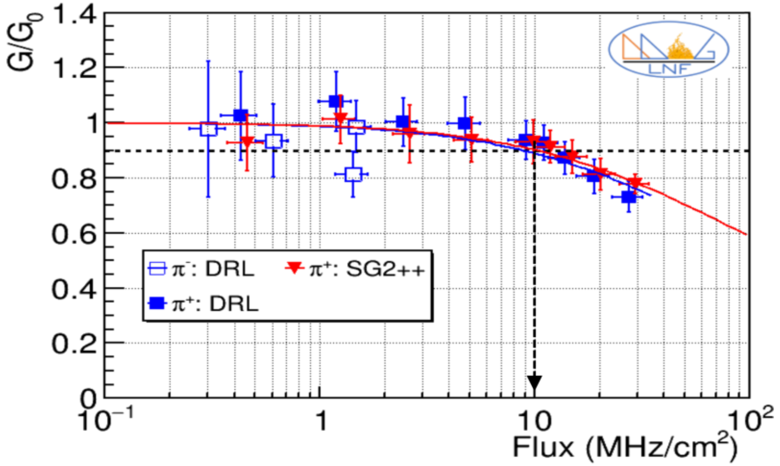

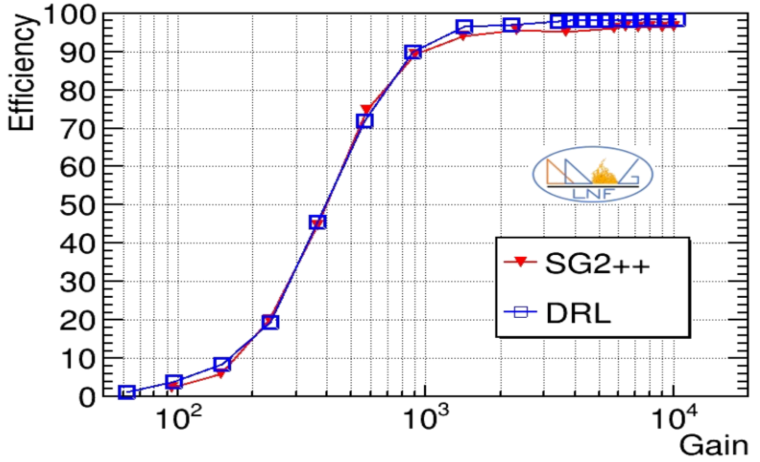

Confronto tra le dimensioni (mm²):

- Pads fisiche attuali delle MWPCs
- Pad delle μRWELL (in rosso)

Reg / Sta	M2	M3	M4	M5
R1	38x31 -> 9x9	41x34 -> 10x10	29x36 -> 11x10	31x39 -> 12x11
R2	76x31 -> 9x18	82x34 -> 10x19	58x73 -> 11x21	62x77 -> 12x22
R3	25x125	27x135	58x145	62x155
R4	50x250	54x270	58x290	62x309

LHCB-TDR-023

The muon mis-IDentification

The **muon identification** acts at different levels:

2. For each IsMuon track candidate, the χ^2_{corr} is calculated, from distances between the extrapolated points and hits on stations
JINST 15 (2020) T12005

$$\chi^2_{corr} \approx \frac{1}{N}\sum_i \left\{ \left(\frac{x_i - x_{track}}{pad_x}\right)^2 + \left(\frac{y_i - y_{track}}{pad_y}\right)^2 \right\}$$

<u>False muon hits</u> can be identified on stations at very crowded environment.

Development of a software to simulate the full hits generation at Run 5, in 25 ns time window :

- New *FoI* definitions
- Different χ^2_{corr} cut

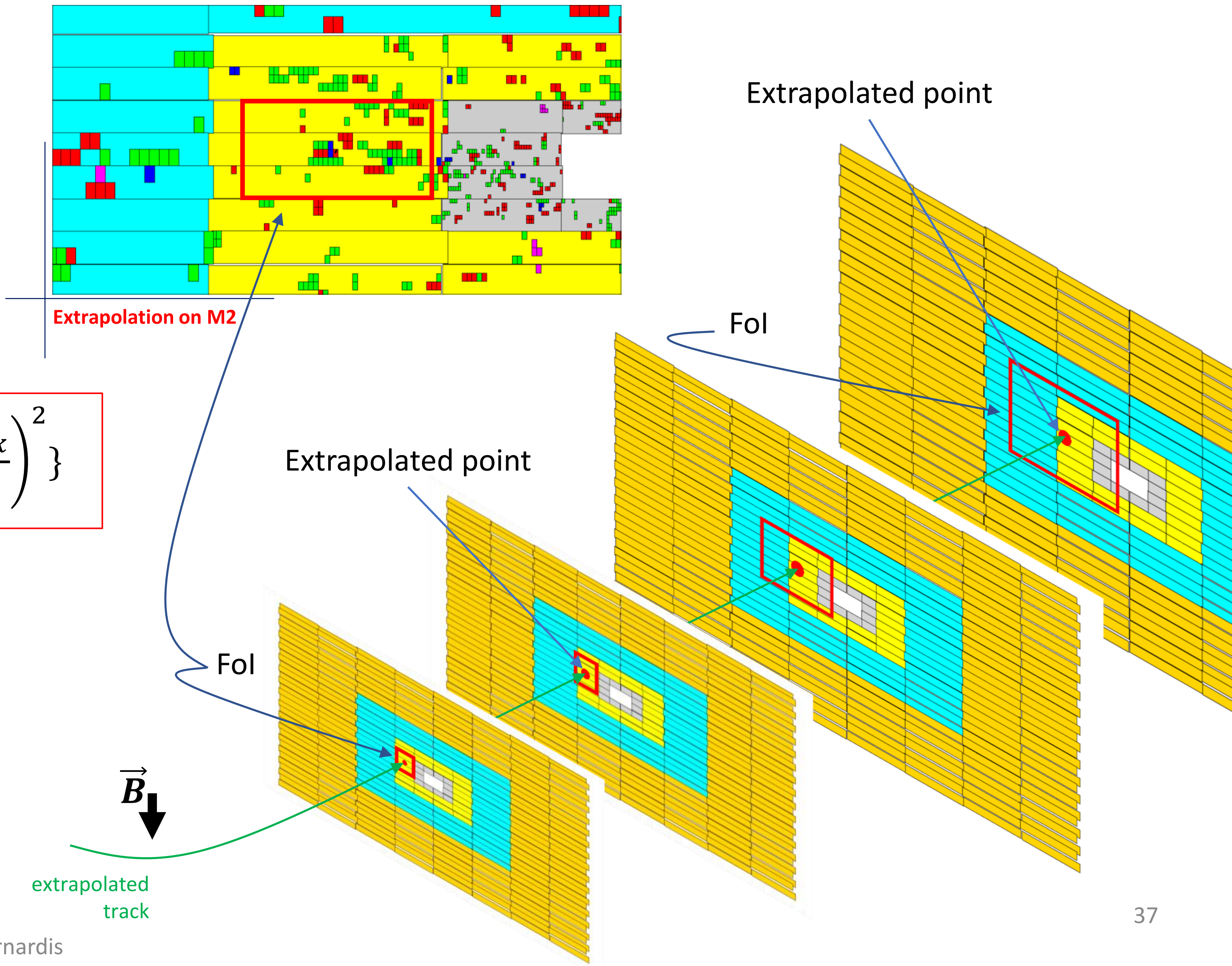

D_s SPECTROSCOPY
In the heavy quark limit model

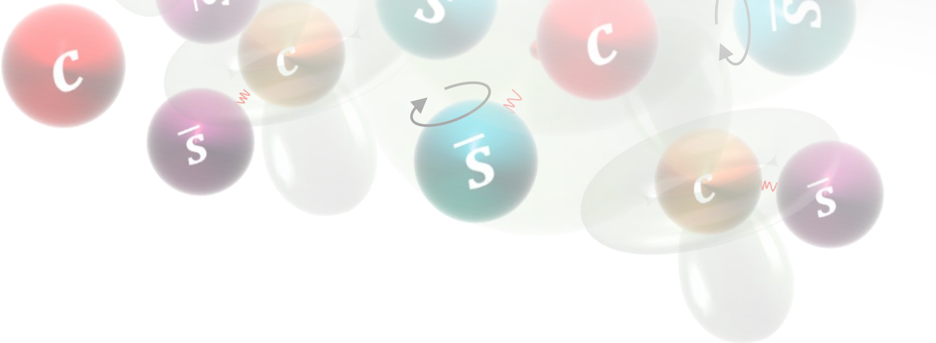

At high energy scale, α_s is small: perturbative interactions and at **short distance scales** $\ll R_{had}$

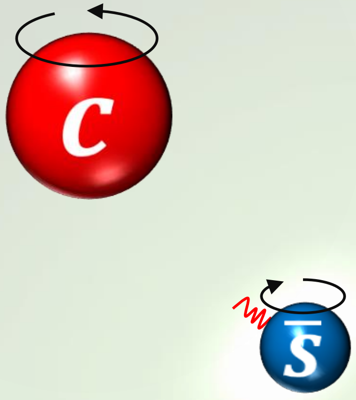

Strong coupling constant

$$\alpha_s(Q^2) \propto \frac{12\pi}{\ln\left(Q^2/\Lambda^2_{\text{QCD}}\right)}$$

$\Lambda_{\text{QCD}} \approx 0.2$ GeV is the energy scale that separates small from large distance scale.

At small energy scale, α_s is large: interactions with non perturbative confinement phenomena of quarks and gluons at **large length scale**

$$R_{had} \sim \frac{1}{\Lambda_{\text{QCD}}} \approx 1 \text{ fm}$$

- The heavy quark is much smaller than the hadron size and it is surrounded by a strongly interacting cloud of light quarks, antiquarks, and gluons with which the light quark interacts.
- The heavy-quark spin effect is not seen by the light quarks, such that the **heavy-quark spin decouples**.

$$m_c \approx 1.3\ GeV/c^2$$
$$m_s \approx 93\ MeV/c^2$$

The P-wave ($L = 1$) states

Phys. Rev. Lett. 66 (1991) 1130
Phys. Rev. D 12 (1975) 147

In the heavy quark limit model

Bounding force depends on the spin-orbit coupling only of the light $\bar{s}$ quark

Excited **P-states ($\vec{L} = 1$)**

$$L + S_{\bar{s}} \nearrow j_{\bar{s}} = 3/2 \quad \searrow j_{\bar{s}} = 1/2 \quad + \quad S_c = 1/2$$

$\nearrow$

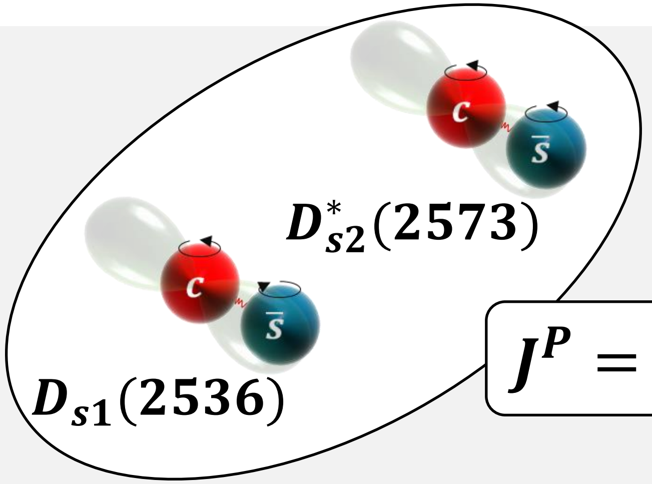

$J^P = 1^+, 2^+$

$\searrow$

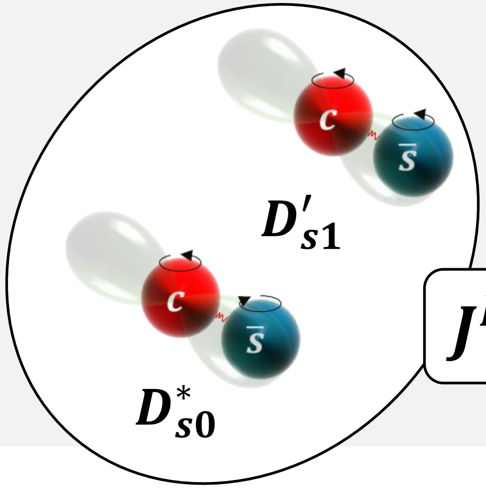

$J^P = 0^+, 1^+$

QCD@Work

D_s SPECTROSCOPY

MESON STATE

$^{2S+1}L_J$

L: orbital angular momentum between constituent quarks (S, P, D correspond to L = 0, 1, 2)

$S = 0, 1$: sum of quark spins

J: total spins of meson state

$j_{\bar{s}}$: sum of L with the spin of light $\bar{s}$ quark

P: parity

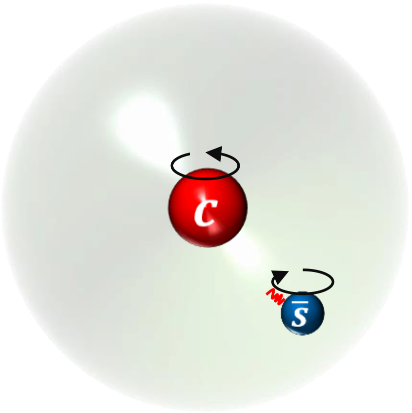

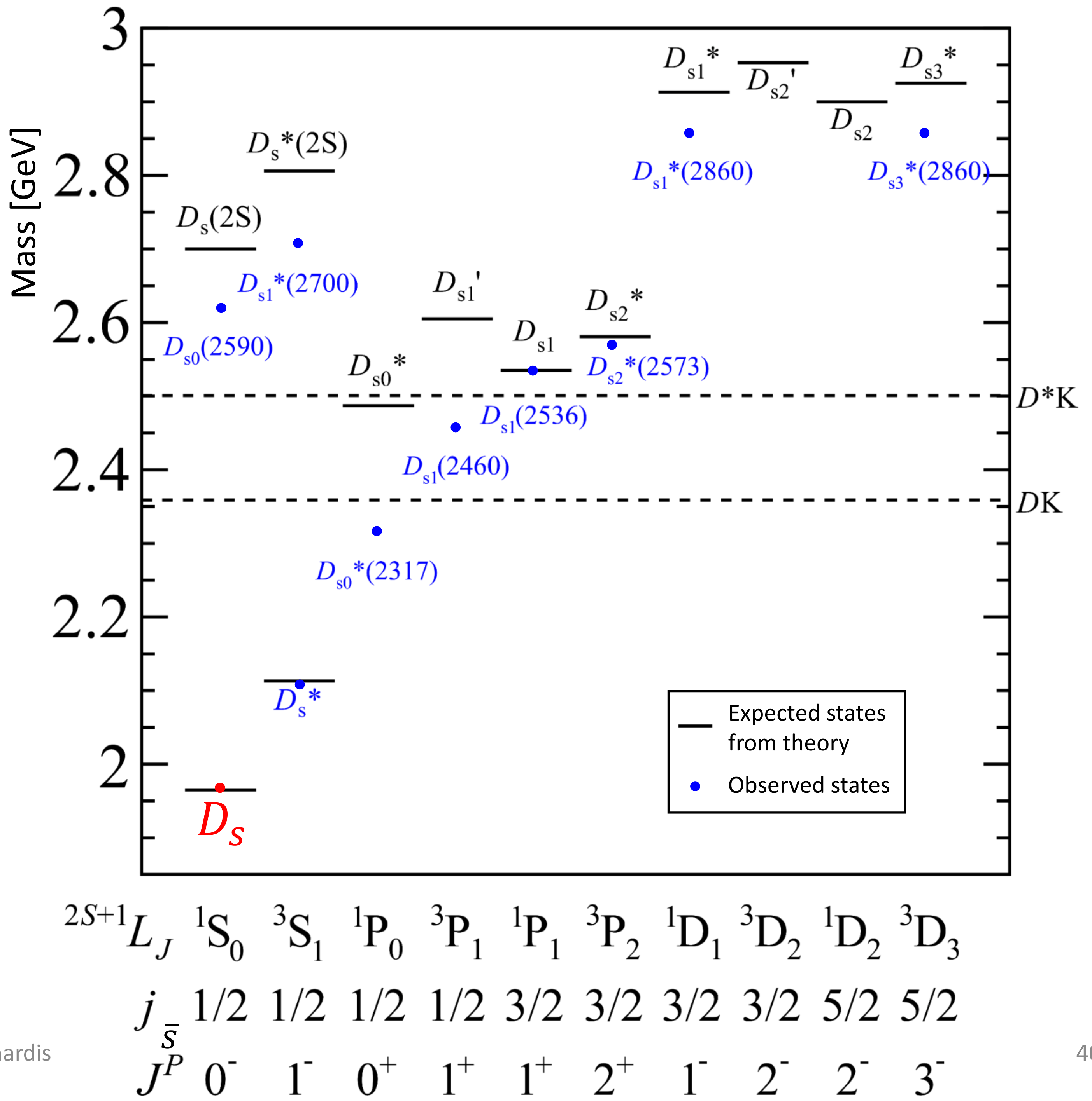

$D_s{}^+\mu^+\mu^-$ selection

Signal and background samples

RUN 2
(2015-2018)
$6\ fb^{-1}$

DATA sample at disposal:

$D_{s1}(2460)^+ \rightarrow D_s{}^+\mu^+\mu^- + c.c.$

$D_{s1}(2460)^+ \rightarrow D_s{}^+\mu^+\mu^+ + c.c$

$D_{s1}(2460)^+ \rightarrow D_s{}^+\mu^-\mu^- + c.c.$

- **D_s candidates:**
  multivariate selection application
- **$D_{s1}(2460)$ candidates:**

  -requirements on D_s mass and PV contraints

  -BDT and BDTG algorithms for signal and background events classifications.

  - **A mixture of four MC samples as signal input**
    (½ for training and ½ for testing)
  - **Wrong Signs sample**
    $m(D_s^+\mu^+\mu^-) < 2600\ MeV/c^2$ used as a proxy of **combinatorial background**
    (½ for training and ½ for testing)

-**PUNZI function** used for BDT cut optimisation

Signal input

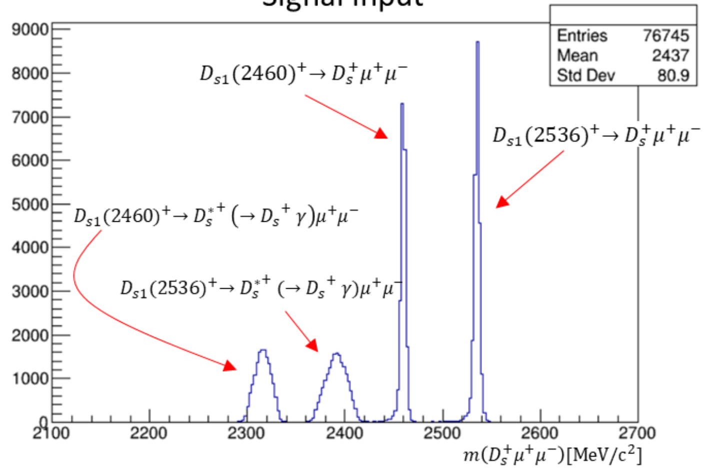

Background input

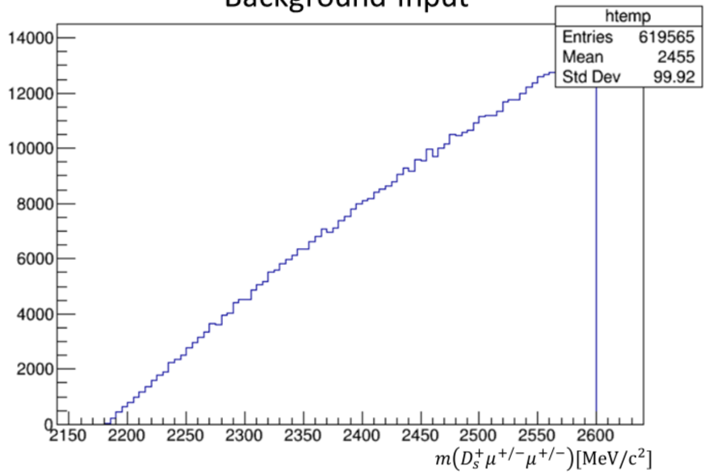

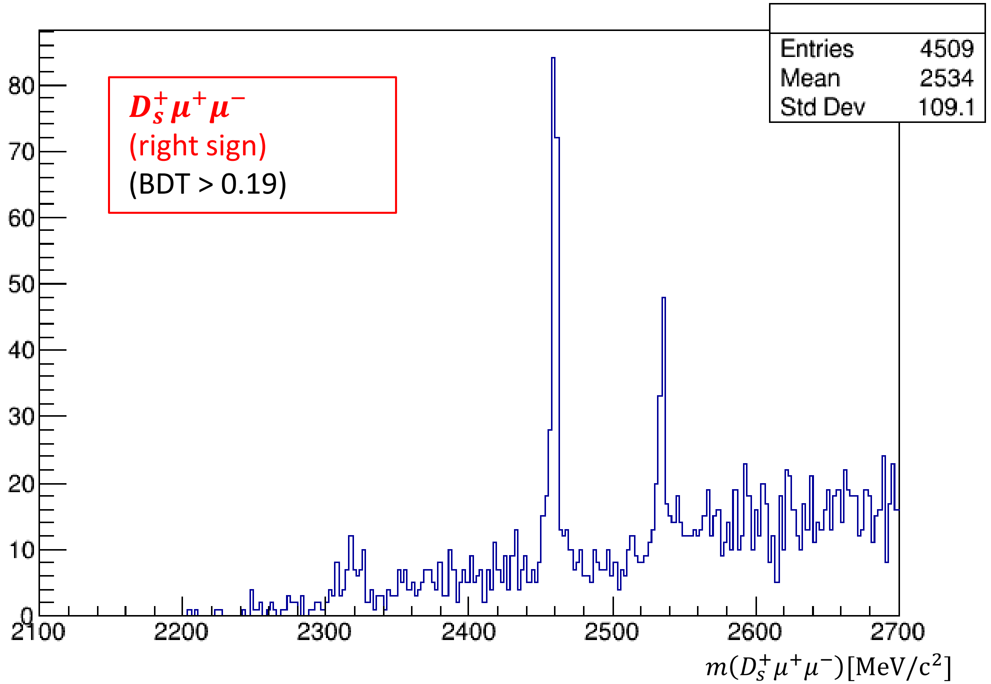

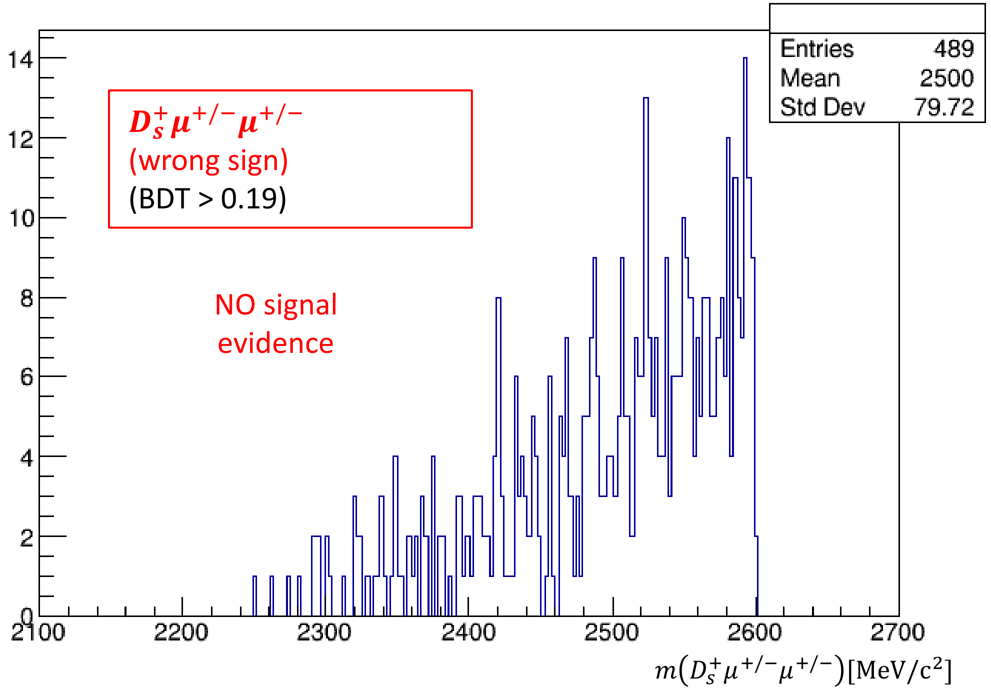

Fit model
(PDF_{total})

RUN 2
(2015-2018)
$6\ fb^{-1}$

$D_{s1}(2460)^+ \rightarrow D_s^+\mu^+\mu^-$

Hypatia ⊗ Breit-Wigner

(M, Γ) floated

Shape fixed to MC

$\sigma_{D_{s1}(2460)}/\sigma_{D_{s1}(2536)}$ fixed to MC

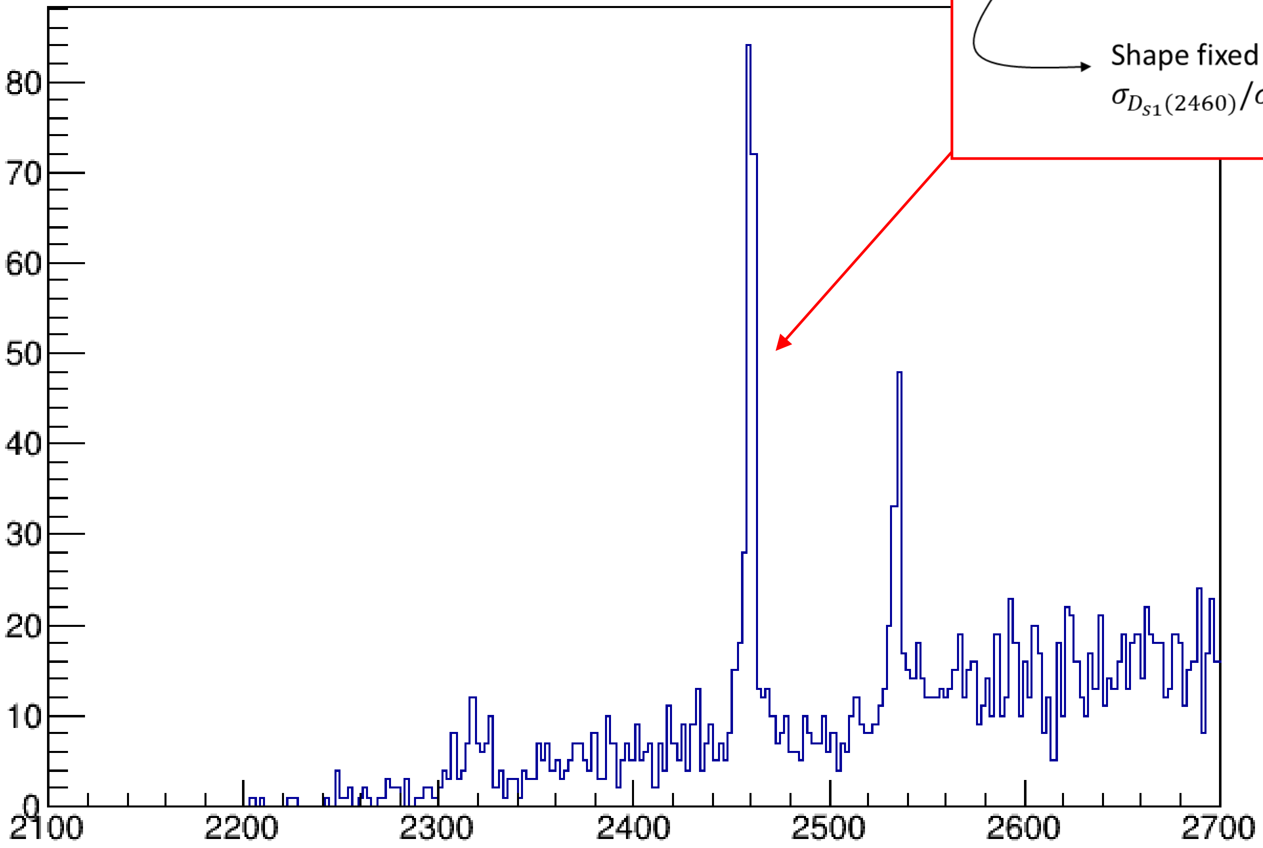

Fit model

(PDF_{total})

RUN 2
(2015-2018)
$6\ fb^{-1}$

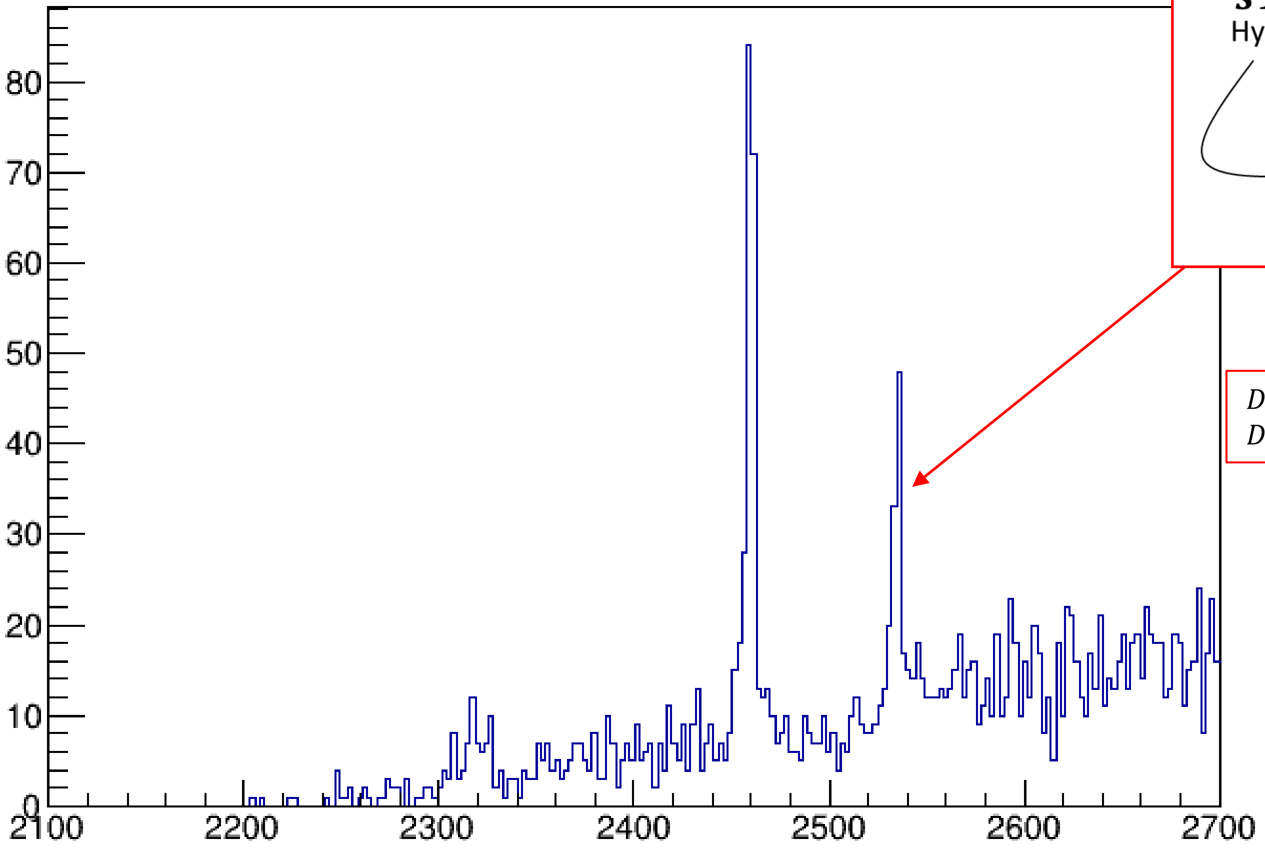

$$D_{s1}(2536)^+ \rightarrow D_s^+ \mu^+ \mu^-$$

Hypatia ⓧ Breit-Wigner

(M, Γ) fixed

Shape fixed to MC
σ float

PDG

$D_{s1}(2536)^{\pm}$	**MASS**	2535.21 ± 0.28 MeV/c^2
$D_{s1}(2536)^{\pm}$	**WIDTH**	0.92 ± 0.05 MeV/c^2

Fit model

(PDF_{total})

RUN 2
(2015-2018)
$6\ fb^{-1}$

$D_{s1}(2460)^+ \rightarrow D_s^{*+}\mu^+\mu^-$

- Shape fixed to MC

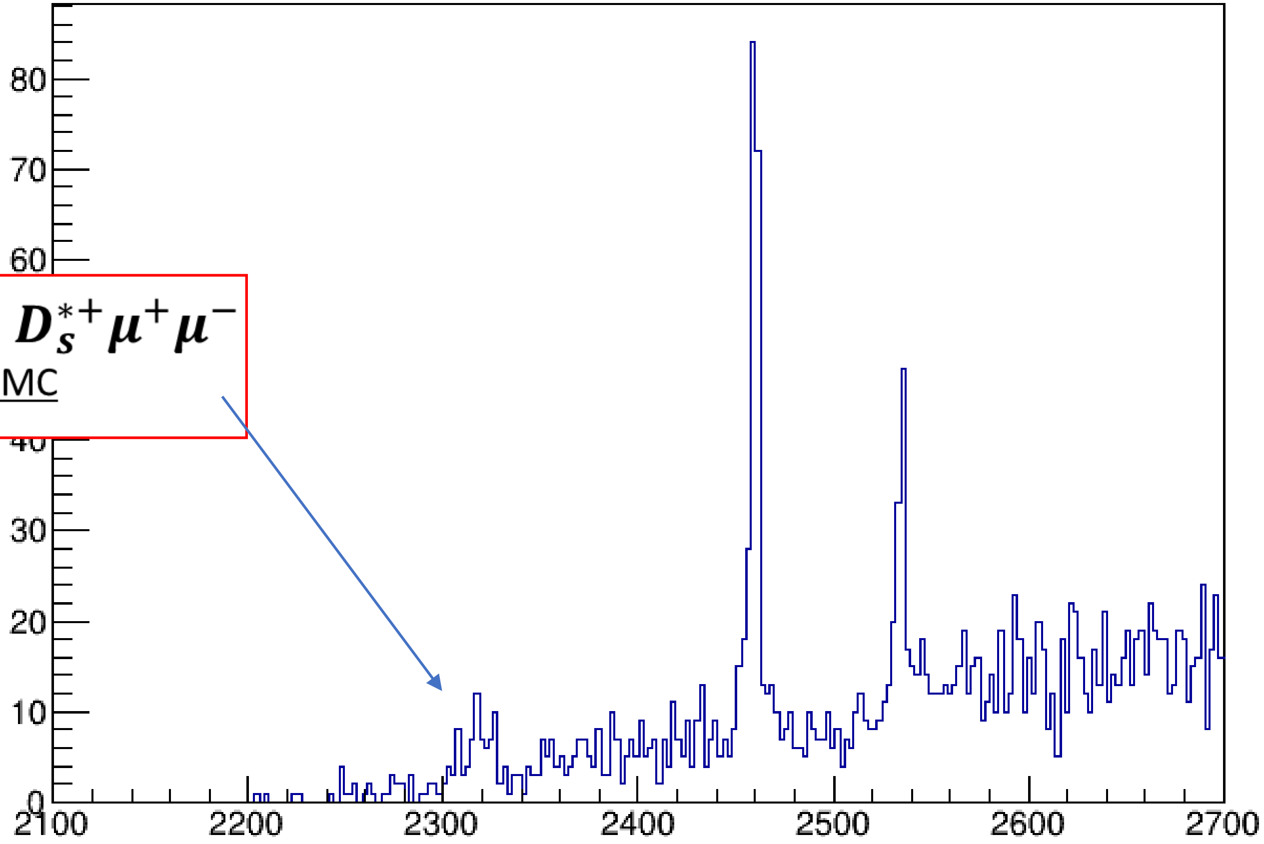

Measurements:

- $m_{D_{s1}(2460)} = 2459.9 \pm 0.2 \quad \mathrm{MeV/c^2}$
- $\Gamma_{D_{s1}(2460)} = \ 0.5 \pm 0.7 \quad \mathrm{MeV/c^2} \quad \sim 0$

log profile likelihood scan at the $\Gamma_{D_{s1}(2460)}$ variation, such to evaluate the upper limit at 95% CL: $\Gamma_{D_{s1}(2460)} < \ 1.77$

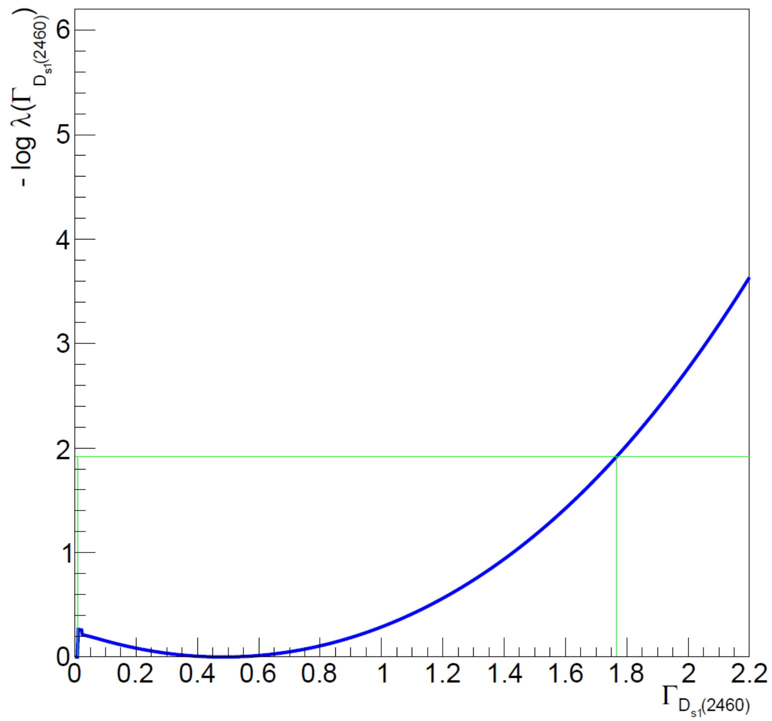

Peak presence associated to the decay events:

$$\boldsymbol{D_{s1}(2460)^+ \rightarrow D_s^{*+}(\rightarrow D_s^{*+}\gamma/\pi^0)\ \mu^+\mu^-}$$

Peak significance estimation is necessary

It is done with the difference of the log-likelihood at minimum between the previous best-fit and the one without the PDF contribution.

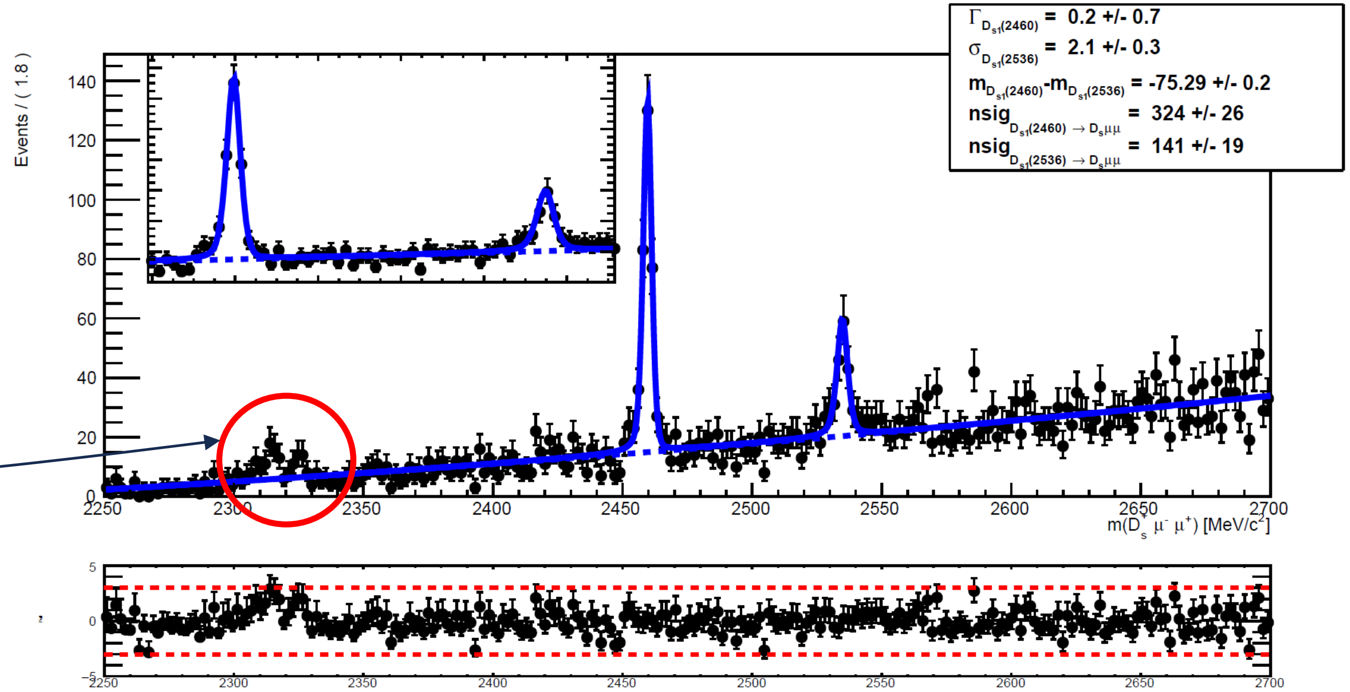

Then: $n_\sigma = 7.7\sigma \ > \ \ 5\sigma$

NEW DECAY OBSERVATION

Francesco Debernardis

Measurements:

Relative branching ratio measurement of:

$$D_{s1}(2460)^+ \to D_s^{*+}(\to D_s^{*+}\gamma/\pi^0)\ \mu^+\mu^-$$

- Trigger constraint application:
  only the Run 2 events satisfying the decay criteria are selected

- Best-fit to triggered data,
  to measure the ratio BR_2460:

$$\text{B\_2460} = \frac{nsig(D_{s1}(2460)^+ \to D_s^{*+}\mu^+\mu^-)}{nsig(D_{s1}(2460)^+ \to D_s^{+}\mu^+\mu^-)} = 0.23 \pm 0.05\ \%$$

- Evaluations of the LHCb reconstruction efficiencies, ϵ_1, ϵ_2 for both $D_{s1}(2460)^+$ decays, by **MC samples**:

$$\epsilon_{1(2)}\left(D_{s1}(2460)^+ \to D_s^{(*)+}\mu^+\mu^-\right) = \frac{\#event\ reconstructed}{\#event\ generated}$$

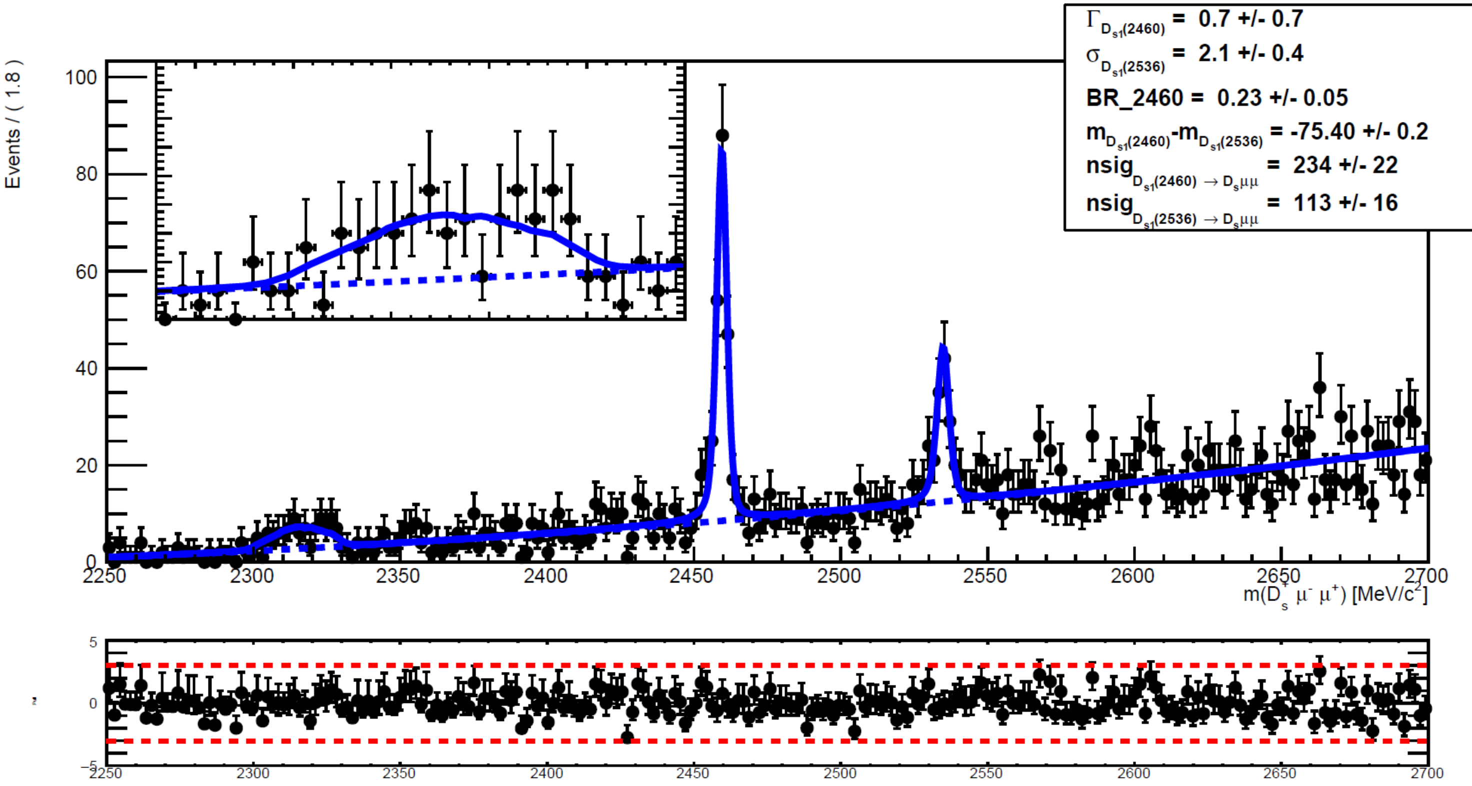

$$\frac{\mathfrak{B}(D_{s1}(2460) \to D_s^*\mu^+\mu^-)}{\mathfrak{B}(D_{s1}(2460) \to D_s\mu^+\mu^-)} = \text{BR\_2460} \cdot \frac{\epsilon_1}{\epsilon_2} = 0.48 \pm 0.10$$

Encouraged to search for the decay signal:

$$D_{s1}(2536) \to D_s^*\mu^+\mu^-$$

Fit result:

RUN 2
(2015-2018)
$6\ fb^{-1}$

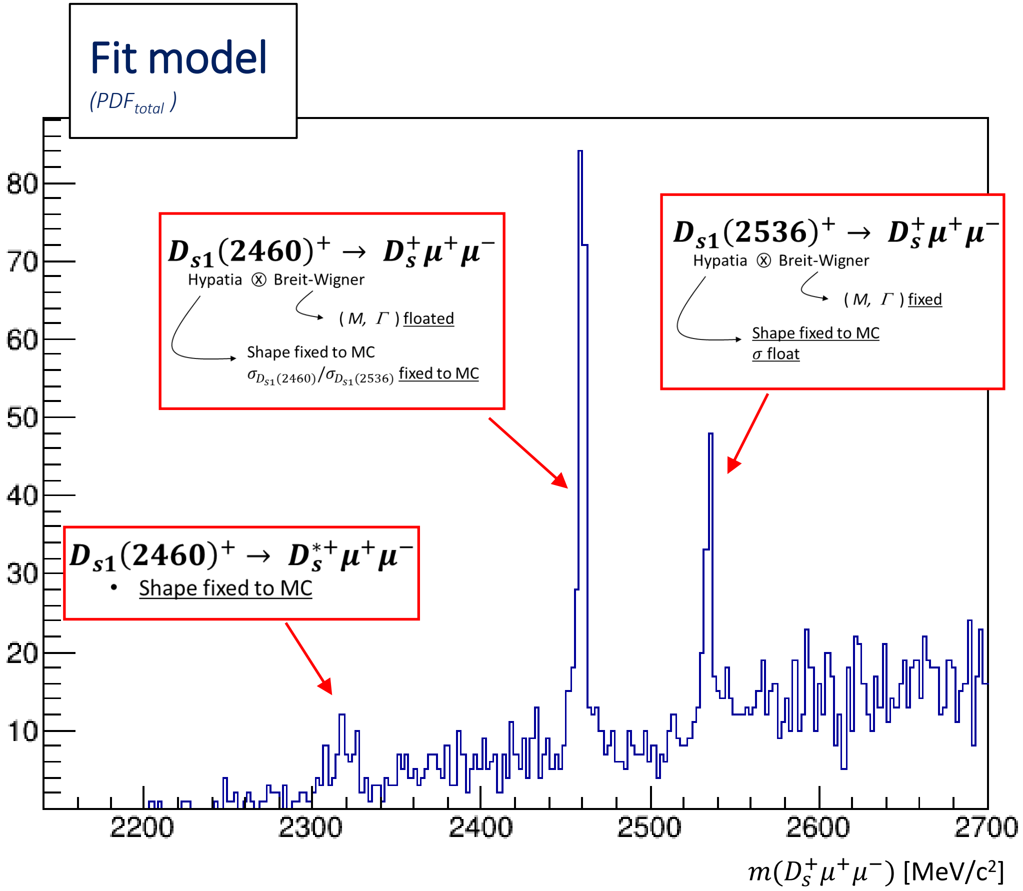

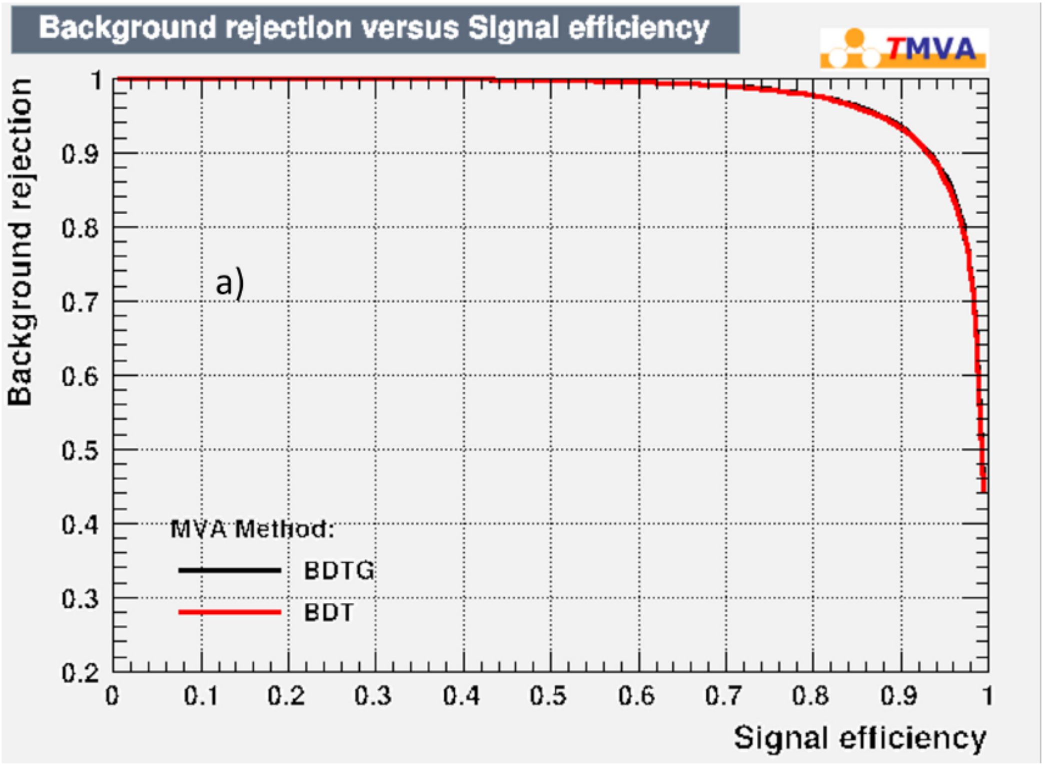

ROC curves from the BDT and the BDTG algorithms used for the multivariate $D_s^+\mu^+\mu^-$ selection. It is evident that the algorithms have about same performance (integral ROC ~ 0.97). However, the BDT classification algorithm is chosen.

Fit model

RUN 2
(2015-2018)
$6\ fb^{-1}$

To add to the PDF_{total}:

$D_{s1}(2536)^+ \rightarrow D_s^{*+}\mu^+\mu^-$
- Shape fixed to MC

$D_{s1}(2460)^+ \rightarrow D_s^{*+}\mu^+\mu^-$
- Shape fixed to MC

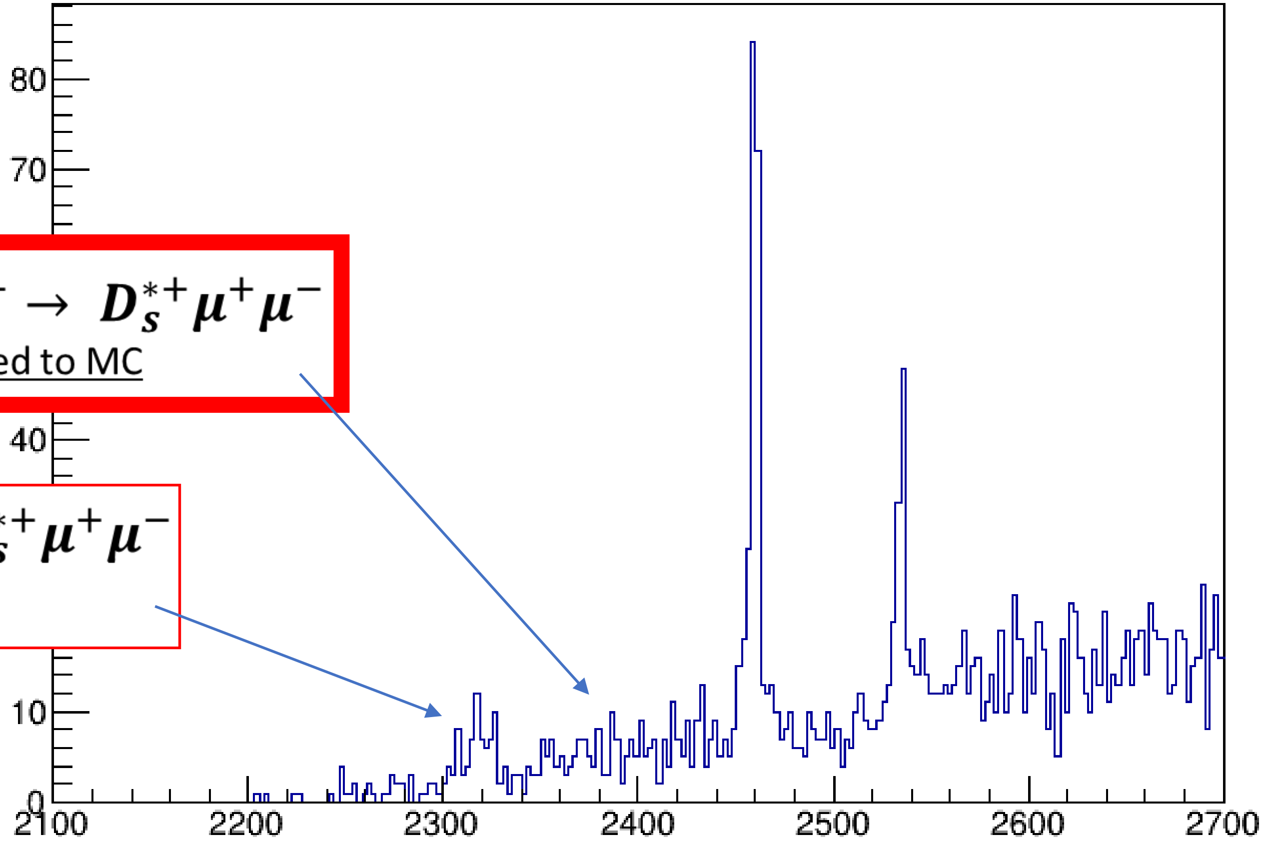

Measurements:

Relative branching ratio measurement of:
$$D_{s1}(2536)^{+} \rightarrow D_s^{*+}(\rightarrow D_s^{*+}\gamma/\pi^0)\,\mu^{+}\mu^{-}$$

- Best-fit to triggered data,
  to measure the ratio BR_2536:

$$B_{2536} = \frac{nsig(D_{s1}(2536)^{+}\rightarrow D_s^{*+}\mu^{+}\mu^{-})}{nsig(D_{s1}(2536)^{+}\rightarrow D_s^{+}\mu^{+}\mu^{-})} = 0.0 \pm 0.1\ \% \ \sim 0$$

- log profile likelihood scan for the upper limit at 95% CL:
  BR_2536 < 0.193

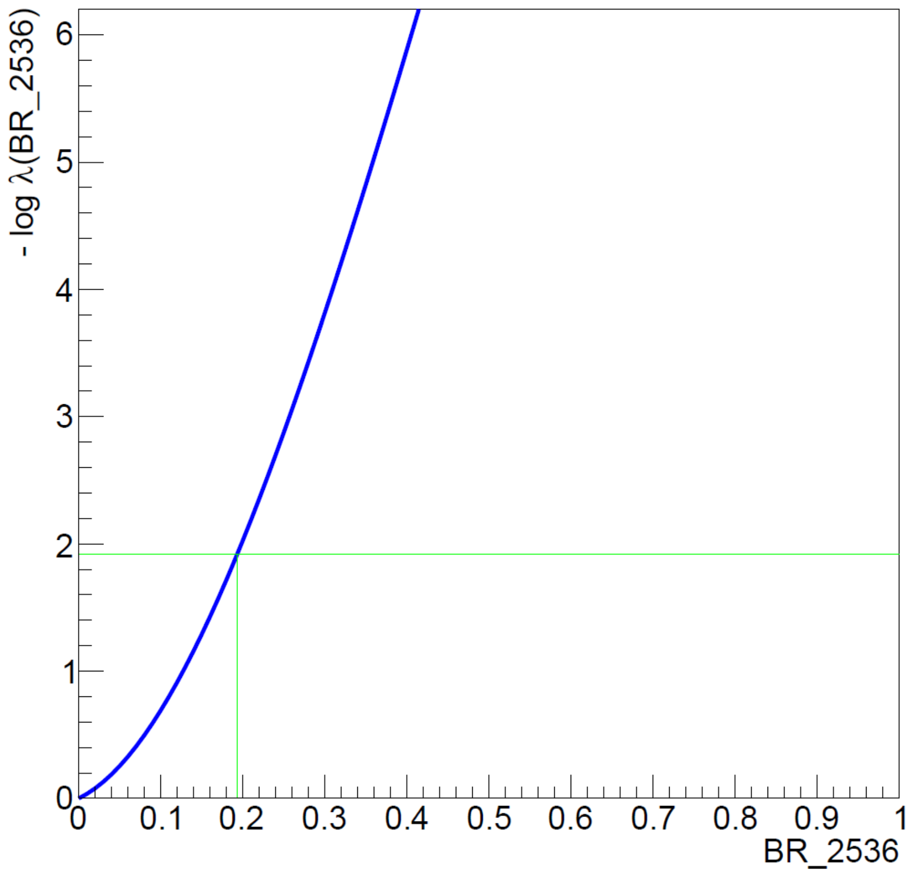

- Evaluations of the LHCb reconstruction efficiencies, ϵ'_1, ϵ'_2 for both $D_{s1}(2536)^{+}$ decays, by **MC samples**:

$$\epsilon'_{1(2)}\left(D_{s1}(2536)^{+} \rightarrow D_s^{(*)+}\mu^{+}\mu^{-}\right) = \frac{\#event\ reconstructed}{\#event\ generated}$$

$$\frac{\mathfrak{B}(D_{s1}(2536) \rightarrow D_s^{*}\,\mu^{+}\mu^{-})}{\mathfrak{B}(D_{s1}(2536) \rightarrow D_s\mu^{+}\mu^{-})} = \mathrm{BR\_2536} \cdot \frac{\epsilon'_1}{\epsilon'_2} < 0.133$$

Summary:

RUN 2
(2015-2018)
$6\ fb^{-1}$

Observation of 3 signals/structures:

- First observation of $D_{s1}(2460) \to D_s\mu^+\mu^-$ decays.
- Evidence/observation of $D_{s1}(2460) \to D_s{}^*\mu^+\mu^-$ decays.
- First observation of the puzzling decay of $D_{s1}(2536) \to D_s\mu^+\mu^-$ despite the **lack of $D_s\gamma$ decay observation**.

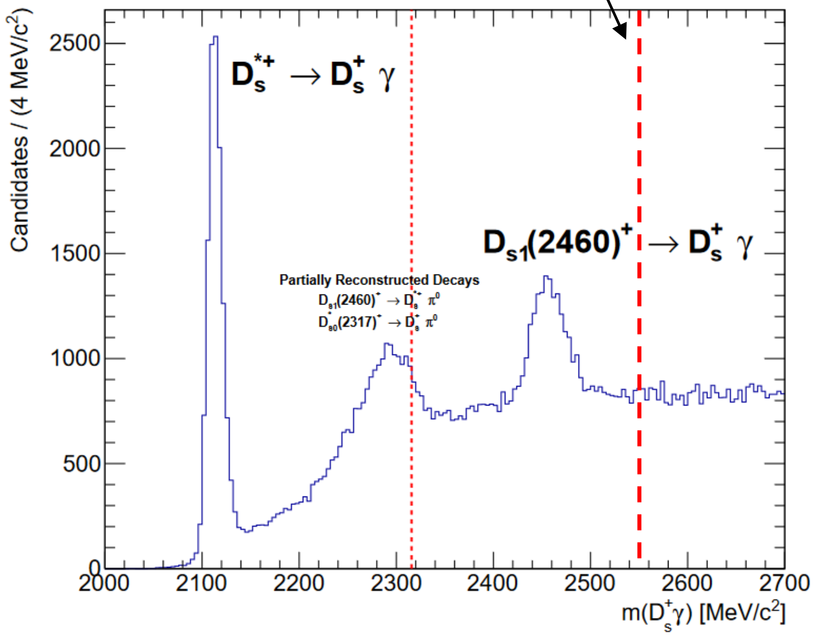

- Radiative decays largely suppressed due to dominance of strong decays to $D^{*+}K^0$ decay mode [PR D 2016, 93.3: 034035]
- $\boldsymbol{D_{s1}(2536)^+ \to D_s^+\eta}$ $(BR(\eta \to \mu^+\mu^-) \cong 6 \cdot 10^{-6})$
  forbidden for the angular momentum conservation:
  $\vec{J}_{D_{s1}(2536)} = \vec{1} = \vec{J}_{final} = \vec{L} + \vec{s}_{D_s} + \vec{s}_\eta = \vec{L}$
  $P_{D_{s1}(2536)} = +1 \neq P_{final} = (-1)(-1)(-1)^L = -1$
- $\boldsymbol{D_{s1}(2536)^+ \to D_s^+\omega}$ $(BR(\omega \to \mu^+\mu^-) \cong 7 \cdot 10^{-5})$
  possible, according to the angular momentum, parity and isospin conservation:
  $\vec{J}_{D_{s1}(2536)} = 1 = \vec{J}_{final} = \vec{L} + \vec{s}_{D_s} + \vec{s}_\omega = \vec{L} + 1$
  $P_{D_{s1}(2536)} = +1 \neq P_{final} = (-1)(-1)(-1)^L = +1$
  } $\vec{L} = 0, 2$
  $I_{D_{s1}(2536)} = 0 = I_{final} = 0 + 0$
- $\boldsymbol{D_{s1}(2536)^+ \to D_s^+\rho}$ $(BR(\rho \to \mu^+\mu^-) \cong 5 \cdot 10^{-5})$
  possible, according to the angular momentum and parity but the isospin conservation:
  $I_{D_{s1}(2536)} = 0 \neq I_{final} = 0 + 1 = 1$

N.B.
$D_{s1}(2460)^+ \to D_s^{*+}\pi^0$
is also an isospin violating decay but $BR \sim 50\%$

The puzzle of the $D_{s1}(2460)$ meson

Surprising observation:
$D_{s1}(2460)^+ \to D_s^{*+}\pi^0$
CLEO (2003)

- mass smaller than all theoretical predictions
- observed in the isospin-violating $D_s^*\pi^0$ channel
- narrow state

Theoretical predictions

- Broad $c\bar{s}$ meson state
- Massive enough that dominant strong decays would have been isospin-conserving in D^*K final states.

Presented at:

EPJ Web Conf. 270 (2022) 00013

$D_{s1}(2460)^+$

decay modes	
$D_s^{*+}\pi^0$	$(48 \pm 11)\%$
$D_s^+\gamma$	$(18 \pm 4)\%$
$D_s^+\pi^+\pi^-$	$(4.3 \pm 1.3)\%$
TOT	$(70 \pm 16)\%$

In a $c\bar{s}$ scenario: isospin-violating decay is suppressed.

For the $D_{s1}(2460)$: isospin-violating decay $D_s^*\pi^0$ is much frequent, suggesting a 4-quarks system ($c\bar{s}u\bar{u}$ or $c\bar{s}d\bar{d}$)

$D_{s1}(2460)^\pm$	**MASS**	2459.5 ± 0.6 MeV/c^2
$D_{s1}(2460)^\pm$	**WIDTH**	< 3.5 MeV/c^2

PDG

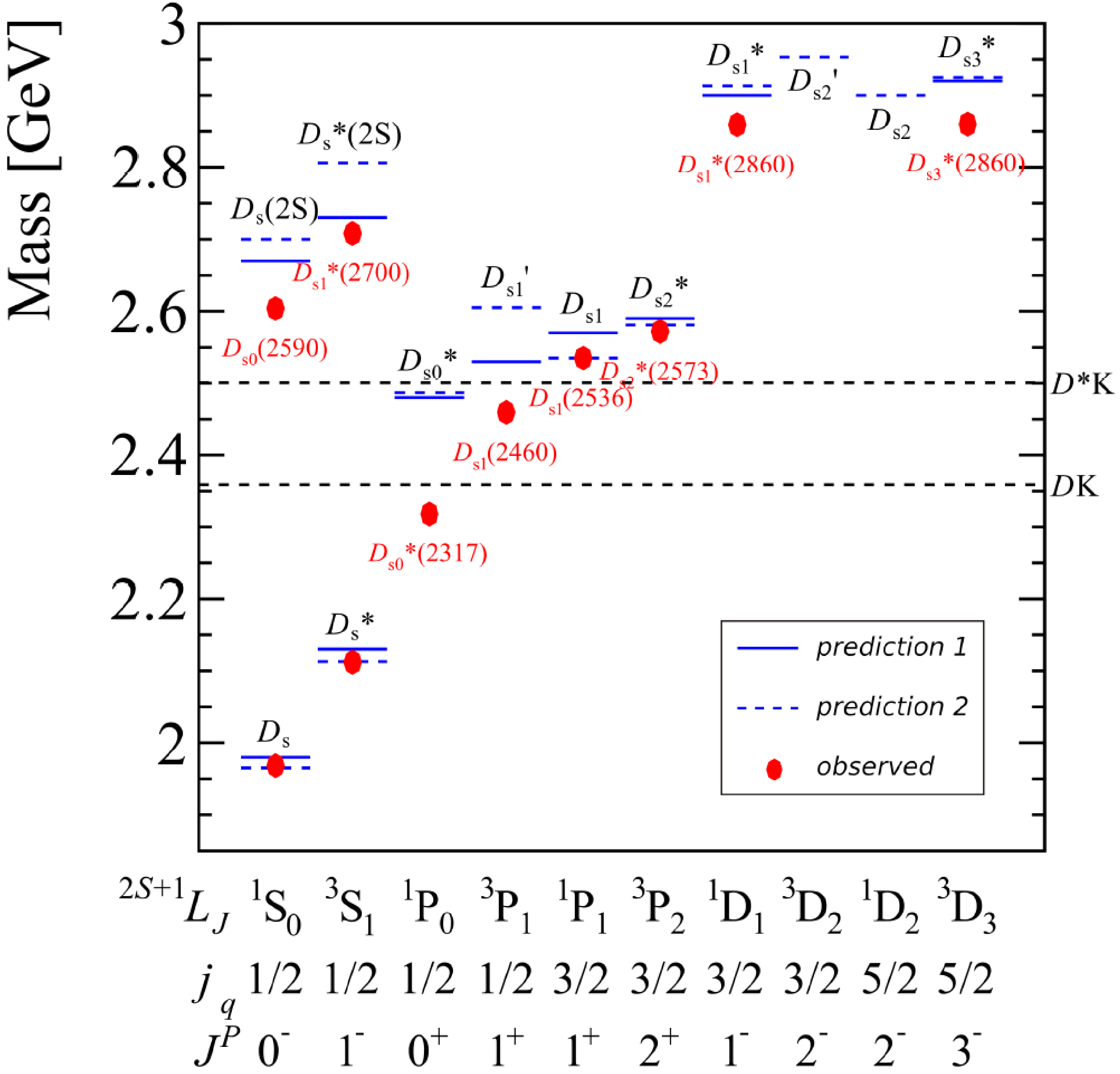
Mass [GeV]
3
2.8
2.6
2.4
2.2
2
D_s
D_s*
D_s(2S)
D_s*(2S)
D_{s0}*
D_{s1}'
D_{s1}
D_{s2}*
D_{s1}*
D_{s2}'
D_{s2}
D_{s3}*
D_{s0}(2590)
D_{s1}*(2700)
D_{s0}*(2317)
D_{s1}(2460)
D_{s1}(2536)
D_{s2}*(2573)
D_{s1}*(2860)
D_{s3}*(2860)
D*K
DK
prediction 1
prediction 2
observed
$^{2S+1}L_J$ $^1S_0$ $^3S_1$ $^1P_0$ $^3P_1$ $^1P_1$ $^3P_2$ $^1D_1$ $^3D_2$ $^1D_2$ $^3D_3$
j_q 1/2 1/2 1/2 1/2 3/2 3/2 3/2 3/2 5/2 5/2
J^P 0^- 1^- 0^+ 1^+ 1^+ 2^+ 1^- 2^- 2^- 3^-

Estimate of rates at Upgrade II

- Run 3 scalers data collected during November 2022, used to extrapolate rate values at the U2 luminosity

- Scaler data: counts of OR-ed bi-gaps
  - collected in 20 sec
  - at 7 different values of luminosity

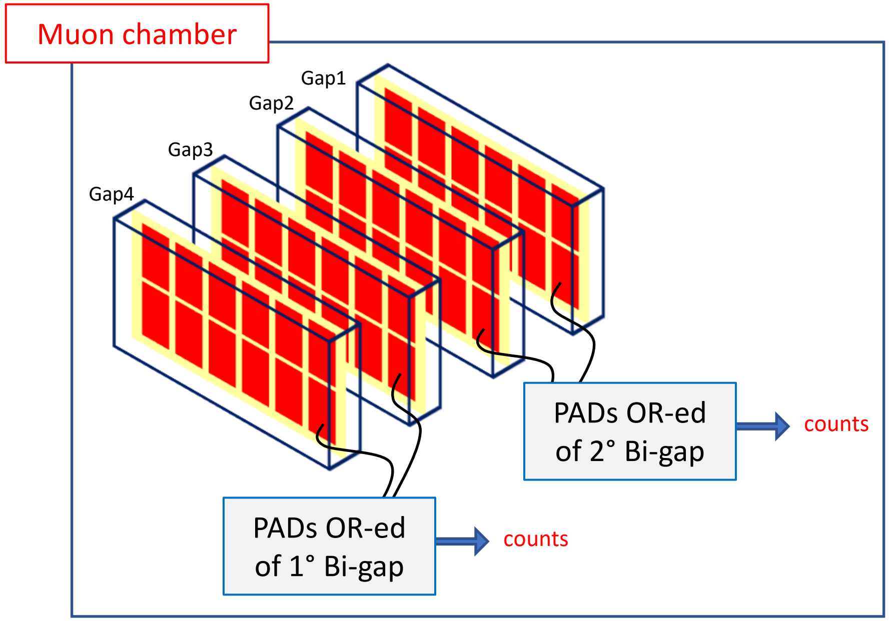

Protons colliding per bunch (μ real):

μ = 1.10	L = $1.05\text{x}10^{32}$ cm^{-2} s^{-1}
μ = 1.45	L = $1.39\text{x}10^{32}$ cm^{-2} s^{-1}
μ = 2.29	L = $2.19\text{x}10^{32}$ cm^{-2} s^{-1}
μ = 2.92	L = $2.79\text{x}10^{32}$ cm^{-2} s^{-1}
μ = 3.50	L = $3.35\text{x}10^{32}$ cm^{-2} s^{-1}
μ = 4.05	L = $3.87\text{x}10^{32}$ cm^{-2} s^{-1}
μ = 4.56	L = $4.36\text{x}10^{32}$ cm^{-2} s^{-1}

Absorber instead of HCAL

LHCB-INT-2019-008

Rates reduction

(~80% of which is background):

M2R1: -42%
M2R2: -69%
M2R3: -64%

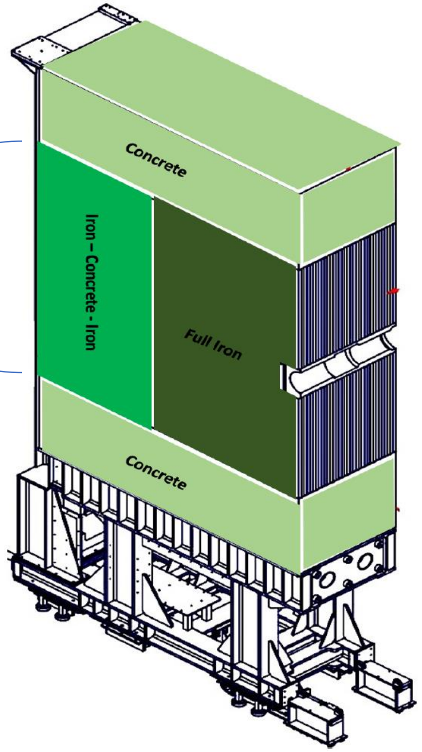

ferro-calcestruzzo-ferro ($6.2\ \lambda_I$), agente su R4 di M2

solo ferro ($10.1\ \lambda_I$), agente su R1-R3 di M2

Calcestruzzo ($4\ \lambda_I$), agente su R4 di M2

μ-ID efficiency loss negligible.

Evaluated with $K_s^0 \to \mu^+\mu^-$ events

	HCAL	Shielding
1μ, all regions	$97.5 \pm 0.2\%$	$97.7 \pm 0.2\%$
R1	$93.1 \pm 0.9\%$	$93.4 \pm 0.8\%$
R2	$98.2 \pm 0.3\%$	$98.7 \pm 0.2\%$
R3	$99.1 \pm 0.2\%$	$97.4 \pm 0.3\%$
R4	$96.9 \pm 0.4\%$	$98.8 \pm 0.2\%$
2μ, all regions	$94.8 \pm 0.4\%$	$95.4 \pm 0.3\%$

Mirrorbor

(under study)

For termal neutrons absorption

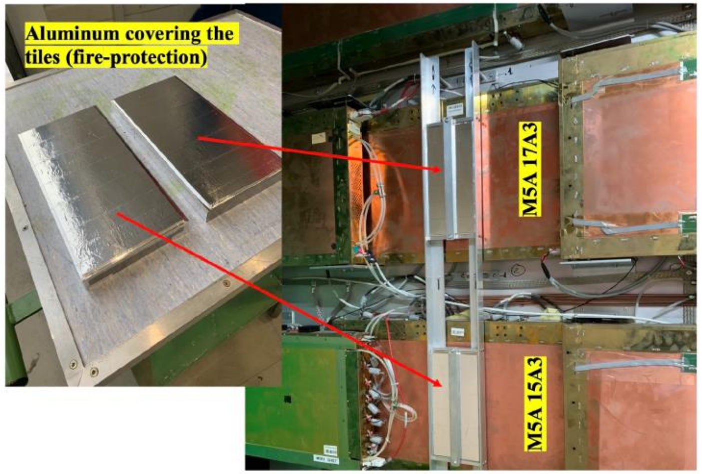

Data usage in the analysis

RUN 2
(2015-2018)
$6\ fb^{-1}$

1. $D_s^{\ +} \to K^+K^-\pi^+ + c.c.$
   Used for $D_s^{\ +}$ decay identification with a multivariate technique

2. $D_{s1}(2460)^+ \to D_s^{\ +}\mu^+\mu^- + c.c.$
   Used for $D_{s1}(2460)^+$ search

3. $D_{s1}(2460)^+ \to D_s^{\ +}\mu^+\mu^+ + c.c.$

4. $D_{s1}(2460)^+ \to D_s^{\ +}\mu^-\mu^- + c.c.$
   Decay channels with wrong signs used for background studies

CHAMBERS

Table 3.1: Parameters of the present (Run 3) LHCb muon detector. Focusing on the chambers readout system, the logical (*L.*) and the physical pads (anodic A., and/or cathodic C.) granularity are also indicated. The latter consisting in anodes (*A.*) and cathodes (*C.*). The chambers areas are expressed in cm^2.

		M2	M3	M4	M5
R1	R1 surface	0.9	1.0	1.2	1.4
	N. chambers	12	12	12	12
	Ch. area	30×25	32.4×27	34.8×29	37.1×30.9
	L. granularity	48×8	48×8	12×8	12×8
	Readout	combined	combined	Cathodes	Cathodes
	A. granularity	48×1	48×1	-	-
	C. granularity	8×8	8×8	12×8	12×8
R2	R1 surface	3.6	4.2	4.8	5.5
	N. chambers	24	24	24	24
	Ch. area	60×25	64.8×27	69.5×29	74.3×30.9
	L. granularity	48×4	48×4	12×4	12×4
	Readout	combined	combined	Cathodes	Cathodes
	A. granularity	48×1	48×1	-	-
	C. granularity	8×8	8×8	12×4	12×4
R3	R1 surface	14.4	16.8	19.3	22.1
	N. chambers	48	48	48	48
	Ch. area	120×25	129.6×27	139×29	148.5×30.9
	L. granularity	48×2	48×2	12×2	12×2
	Readout	Cathodes	Cathodes	Cathodes	Cathodes
	A. granularity	-	-	-	-
	C. granularity	48×2	48×2	24×2	24×2
R4	R1 surface	57.7	67.2	77.4	88.3
	N. chambers	192	192	192	192
	Ch. area	120×25	129.6×27	139×29	148.5×30.9
	L. granularity	24×1	24×1	6×1	6×1
	Readout	Anodes	Anodes	Anodes	Anodes
	A. granularity	24×1	24×1	24×1	24×1
	C. granularity	-	-	-	-

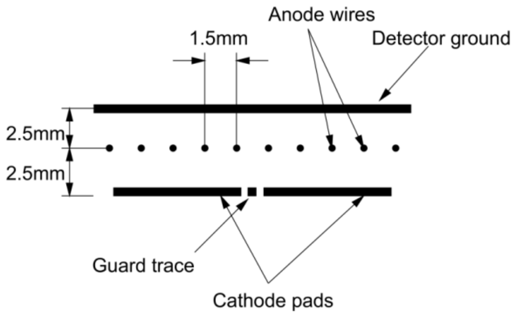

Table 3.2: Cathodes and anodes size, in mm^2, in the present (Run 3) muon detector where present.

		M2	M3	M4	M5
R1	Anodes	6.3 × 250	6.7 × 270	-	-
	Cathodes	38 × 31	41 × 34	29 × 36	31 × 39
R2	Anodes	12.5 × 250	13.5 × 270	-	-
	Cathodes	76 × 31	82 × 34	58 × 73	62 × 77
R3	Anodes	-	-	-	-
	Cathodes	25 × 125	27 × 135	58 × 145	62 × 155
R4	Anodes	50 × 250	54 × 270	58 × 290	62 × 309
	Cathodes	-	-	-	-

Detector performances till now:

- *Geometrical acceptance:* $10 < \theta < 300/250$ mrad (bending/non bending plane)
- *p* measurement resolution: $\Delta p/p$= 0,5% / 1,0% at low momentum / at 200 GeV/c
- *Impact parameter* resolution: (15 + 29/p_T[GeV]) μm
- *Track reconstruction* resolution: 96% for long tracks
- *Muon identification* efficiency: $\approx$ 97%